




OPEN ACCESS

## TRANSLATIONAL SCIENCE

# Acod1-mediated inhibition of aerobic glycolysis suppresses osteoclast differentiation and attenuates bone erosion in arthritis

Katerina Kachler,<sup>1,2</sup> Darja Andreev,<sup>1,2,3</sup> Shreeya Thapa,<sup>1,2</sup> Dmytro Royzman,<sup>4</sup> Andreas Gießl,<sup>5</sup> Shobika Karuppusamy,<sup>1,2</sup> Mireia Llerins Perez ,<sup>1,2</sup> Mengdan Liu,<sup>1,2,6</sup> Jörg Hofmann,<sup>7</sup> Arne Gessner,<sup>8</sup> Xianyi Meng,<sup>1,2</sup> Simon Rauber ,<sup>1,2</sup> Alexander Steinkasserer,<sup>4</sup> Martin Fromm,<sup>8</sup> Georg Schett ,<sup>1,2</sup> Aline Bozec ,<sup>1,2</sup>

**Handling editor** Rik Jozef Urbain Lories

► Additional supplemental material is published online only. To view, please visit the journal online (<https://doi.org/10.1136/ard-2023-224774>).

For numbered affiliations see end of article.

**Correspondence to**

Professor Aline Bozec, Department of Internal Medicine 3 Rheumatology and Immunology, Friedrich-Alexander University Erlangen-Nuremberg, Erlangen 91054, Germany; [aline.bozec@uk-erlangen.de](mailto:aline.bozec@uk-erlangen.de)

Received 25 July 2023

Accepted 20 June 2024

**ABSTRACT**

**Objectives** Metabolic changes are crucially involved in osteoclast development and may contribute to bone degradation in rheumatoid arthritis (RA). The enzyme aconitate decarboxylase 1 (Acod1) is known to link the cellular function of monocyte-derived macrophages to their metabolic status. As osteoclasts derive from the monocyte lineage, we hypothesised a role for Acod1 and its metabolite itaconate in osteoclast differentiation and arthritis-associated bone loss.

**Methods** Itaconate levels were measured in human peripheral blood mononuclear cells (PBMCs) of patients with RA and healthy controls by mass spectrometry. Human and murine osteoclasts were treated with the itaconate derivative 4-octyl-itaconate (4-OI) in vitro. We examined the impact of Acod1-deficiency and 4-OI treatment on bone erosion in mice using K/BxN serum-induced arthritis and human TNF transgenic (hTNFtg) mice. SCENITH and extracellular flux analyses were used to evaluate the metabolic activity of osteoclasts and osteoclast progenitors. Acod1-dependent and itaconate-dependent changes in the osteoclast transcriptome were identified by RNA sequencing. CRISPR/Cas9 gene editing was used to investigate the role of hypoxia-inducible factor (Hif)-1 $\alpha$  in Acod1-mediated regulation of osteoclast development.

**Results** Itaconate levels in PBMCs from patients with RA were inversely correlated with disease activity. Acod1-deficient mice exhibited increased osteoclast numbers and bone erosion in experimental arthritis while 4-OI treatment alleviated inflammatory bone loss in vivo and inhibited human and murine osteoclast differentiation in vitro. Mechanistically, Acod1 suppressed osteoclast differentiation by inhibiting succinate dehydrogenase-dependent production of reactive oxygen species and Hif1 $\alpha$ -mediated induction of aerobic glycolysis.

**Conclusion** Acod1 and itaconate are crucial regulators of osteoclast differentiation and bone loss in inflammatory arthritis.

**INTRODUCTION**

Rheumatoid arthritis (RA) is a chronic inflammatory joint disease that affects up to 1% of the population.<sup>1</sup> The key feature of RA is synovial inflammation, which is characterised by the activation of fibroblast-like synoviocytes, neovascularisation and immune cell infiltration, resulting in an

**WHAT IS ALREADY KNOWN ON THIS TOPIC**

⇒ The pathogenesis of rheumatoid arthritis (RA) is commonly linked to metabolic dysregulation, yet the metabolic profile of osteoclasts in RA, along with the factors responsible for potential changes, remain poorly defined.

**WHAT THIS STUDY ADDS**

⇒ Acod1 and itaconate counteract the metabolic changes driving osteoclast overactivation in RA, including Hif1 $\alpha$ -mediated induction of aerobic glycolysis, mitochondrial hyperpolarisation and mitochondrial repurposing for ROS formation.

**HOW THIS STUDY MIGHT AFFECT RESEARCH, PRACTICE OR POLICY**

⇒ Insights into how Acod1 and itaconate affect osteoclast metabolism could advance our understanding of RA-associated bone loss and inspire novel therapeutic strategies.

overall expansion of the synovial membrane.<sup>2</sup> The phenotypic traits that are linked to synovial hyperplasia, such as cellular dedifferentiation, sustained proliferation and tissue invasion impose extensive nutritional demands on immune and stromal cells.<sup>3</sup> The microenvironment of inflammatory joint lesions is furthermore defined by low oxygen and nutrient availability, enforcing additional bioenergetic changes on resident cells.<sup>4,5</sup> To understand the implications of metabolic dysregulation on disease development, extensive research has focused on identifying inflammation-related metabolic adaptations in RA-associated cells over the last decade. These studies revealed that although RA-specific metabolic profiles vary across different cell types, they are consistently linked to enhanced cell pathogenicity, signifying metabolic reprogramming as an important contributing factor for RA progression rather than a mere consequence of the hypoxic and nutrient-deprived microenvironment of the joint.<sup>6–8</sup>

Another important hallmark of RA, besides synovial inflammation, is enhanced bone degradation. It can manifest as local erosion of bone tissue within the inflamed joint, periarticular bone loss that occurs in close proximity to the inflamed tissue area and



© Author(s) (or their employer(s)) 2024. Re-use permitted under CC BY-NC. No commercial re-use. See rights and permissions. Published by BMJ.

**To cite:** Kachler K, Andreev D, Thapa S, et al. *Ann Rheum Dis* Epub ahead of print: [please include Day Month Year]. doi:10.1136/ard-2023-224774

systemic osteoporosis of the axial and appendicular skeleton.<sup>9–11</sup> Local damage in the articular tissue limits joint mobility and can cause joint destruction while the generalised bone loss puts patients with RA at a higher risk of bone fracture.<sup>10</sup> Osteoclasts, which are the only cells in the body capable of bone degradation, are primarily responsible for all types of RA-associated bone erosion.<sup>12–13</sup> Similar to inflammation, osteoclast mediated bone resorption is a highly energy-demanding process that is sensitive to metabolic modification. Accordingly, osteoclast differentiation is associated with active metabolic reprogramming that involves enhanced mitochondrial biogenesis as well as increased oxygen consumption and glycolytic activity.<sup>14–15</sup> Although the decisive role of metabolic reprogramming for osteoclast development and function has been established, is it still unclear how these dynamic changes are coordinated and translated into specific cellular functions. Moreover, the metabolic profile of osteoclasts and osteoclast precursors (OCPs) in the presence of RA is largely uncharacterised.

The mitochondrial enzyme aconitate decarboxylase 1 (Acod1, also known as immune responsive gene 1 (Irg1)) serves as a mediator between the metabolic condition and the functional state of different types of cells (eg, macrophages and monocytes). It catalyses the production of the tricarboxylic acid cycle intermediate itaconate and is induced in response to numerous stimuli (eg, lipopolysaccharide (LPS) or CpG DNA) that are related to stress, inflammation, infection or tissue damage.<sup>16–18</sup> Itaconate has emerged as a multifunctional immunoregulatory metabolite with primarily anti-inflammatory activity. Its functional mechanisms include the stabilisation of the immunosuppressive transcription factor nuclear factor erythroid 2-like 2 (Nfe2l2, also known as Nrf2), the suppression of aerobic glycolysis through inactivation of glyceraldehyde 3-phosphate dehydrogenase (Gapdh) as well as competitive inhibition of the enzyme succinate dehydrogenase (Sdh).<sup>19–22</sup> More recently, itaconate was also suggested to act as a negative regulator of osteoclast development. 4-octyl-itaconate (4-OI), a cell permeable derivative of itaconate, enhanced Nrf2 activity by inhibition of the E3 ubiquitin ligase Hrd1 in bone marrow-derived macrophages (BMDMs) and was able to suppress osteoclast differentiation *in vitro* and ovariectomy-induced bone loss *in vivo*.<sup>23</sup> However, the link between the Acod1-itaconate axis and the metabolic state of osteoclasts as well as their influence on bone erosion in inflammatory arthritis is unknown. The aim of this study was, therefore, the analysis of Acod1-dependent reprogramming of osteoclast metabolism in the context of bone loss in inflammatory arthritis.

## METHODS

### Human samples

Peripheral blood mononuclear cells (PBMCs) were taken from patients with RA that fulfil the 2010 defined RA classification criteria of the American College of Rheumatology/European League Against Rheumatism.<sup>24</sup> The following analyses were carried out: (1) osteoclast-differentiation assays with tartrate-resistant acid phosphatase (TRAP) staining in 11 patients with RA (8 females, 3 males; mean±SD age: 55±10 years) and 10 healthy controls (8 females, 2 males; mean±SD age: 51±14 years); (2) RNA extraction and qPCR in 21 patients with RA (all females; mean±SD age: 57±10 years) and 15 healthy subjects (13 females, 2 males; mean±SD age: 48±6 years); (3) extracellular flux assays in 3 patients with RA (1 female, 2 males; mean±SD age: 49±7 years) and 4 healthy subjects (3 females, 1 male; mean±SD age: 32±22 years); (4) itaconate

measurement using mass spectrometry in 21 patients with RA (donors were female; mean±SD age: 57±11 years) and 10 healthy donors (donors were female; mean±SD age: 47±5 years). Disease activity of RA was measured by DAS28. Healthy controls and RA patients provided written informed consent for the study.

### Human osteoclast *in vitro* differentiation

PBMCs were isolated from EDTA blood of healthy donors and patients with RA using a Ficoll gradient (Lymphoflot, Bio-Rad). Cells were plated at a cell density of  $3 \times 10^6$ /mL in adhesion medium, composed of  $\alpha$ MEM+GlutaMAX with 1% fetal calf serum (FCS) and 1% penicillin/streptomycin (PS) and incubated at 37°C and 5.5% CO<sub>2</sub> for 1.5 hours to purify monocytes by plastic adhesion. Non-adherent cells were subsequently removed together with the supernatant and the adherent cells were washed and supplemented with OC-medium ( $\alpha$ MEM+GlutaMax with 10% FCS and 1% PS), containing 30 ng/mL macrophage colony-stimulating factor (M-CSF), 2 ng/mL receptor activator of nuclear factor  $\kappa$ B ligand (RANKL) and 1 ng/mL transforming growth factor- $\beta$  (TGF- $\beta$ ) (all Peprotech) to a cell density of  $1.5 \times 10^6$ /mL. Cells were cultured at 37°C and 5.5% CO<sub>2</sub> for 7–10 days until maturation. The assay was terminated on the same day for each pair of matched donors. Medium was exchanged on day 3, day 5 and day 7 of cell culture. Osteoclast differentiation was evaluated by TRAP staining using the acid phosphatase leucocyte kit (Sigma-Aldrich). Stimulation with indicated doses of 4-OI (Cayman Chemical) started on day 3 of osteoclast cell culture and was repeated with each medium exchange. Images were acquired with the All-in-One Fluorescence Microscope BZ-X710 (KEYENCE) and quantification of osteoclast number was performed with ImageJ.

### Extracellular flux analyses with human cells

$4 \times 10^5$  PBMCs were plated in Seahorse XF96 Cell Culture Microplates (Agilent Technologies) in 200  $\mu$ L of adhesion medium and incubated at 37°C and 5.5% CO<sub>2</sub> for 1.5 hours to purify monocytes by plastic adhesion. Non-adherent cells were subsequently removed and the adherent cells were washed and supplemented with 200  $\mu$ L of OC-medium for osteoclast differentiation. For 4-OI stimulation, 50  $\mu$ M 4-OI was added on day 2 of cell culture for 24 hours. Glycolysis and Cell Mito Stress Tests were performed on day 3 of osteoclast *in vitro* differentiation and adenosine triphosphate (ATP) Rate Assay was performed on days 0–10 of cell culture according to manufacturer's instructions. Seahorse XF RPMI Medium (Agilent Technologies) was supplemented with 2 mM L-glutamine (Agilent Technologies) for the Glycolysis Stress Test and with 10 mM glucose, 1 mM pyruvate and 2 mM L-glutamine (Agilent Technologies) for the ATP Rate Assay as well as the Cell Mito Stress Test. The final concentrations of the utilised metabolic compounds were as follows: 10 mM glucose, 2  $\mu$ M oligomycin A, 50 mM 2-deoxy-D-glucose (2-DG), 2  $\mu$ M carbonyl cyanide 4-(trifluoromethoxy) phenylhydrazone (FCCP), 1  $\mu$ M rotenone and 1  $\mu$ M antimycin A (all from Sigma-Aldrich). Extracellular acidification rate (ECAR) and oxygen consumption rate (OCR) were measured in a 96-well XF Extracellular Flux Analyzer (Agilent Technologies) and data were obtained using the Seahorse Wave Desktop Software (Agilent Technologies). Changes in ECAR and in OCR values were used to calculate glycolytic and mitochondrial parameters via Microsoft Excel.

## Mice

C57BL/6NJ-Acod1<sup>em1(IMPC)</sup>/J mice (stock #029340) were initially purchased from Jackson Laboratories, bred with C57BL/6NRj mice (from Janvier Labs) and maintained in the local animal facility. Wild-type (WT) C57BL/6NRj mice were co-housed with C57BL/6NJ-Acod1<sup>em1(IMPC)</sup>/J mice for at least 1 week prior to the start of experiments. Human TNF transgenic (hTNFtg) mice (strain Tg197 on C57BL/6 background) were previously described.<sup>25</sup> Arthritis evaluation was performed twice a week. Littermates were used as controls for the hTNFtg experiments. All mice were housed in a temperature-controlled and humidity-controlled facility with free access to food and water.

## K/BxN serum-induced arthritis

Mice aged 7–9 weeks were injected intraperitoneally with 150  $\mu$ L pooled serum from adult, arthritic K/BxN mice as previously described.<sup>26</sup> Development and progression of arthritis were monitored using a semiquantitative scoring system (0–4 per paw; maximum score of 16).<sup>27</sup> Mice were sacrificed for ex vivo analyses on day 9 post K/BxN serum transfer.

## 4-OI in vivo treatment

For the K/BxN SIA model, 4-OI treatment was conducted on days 1, 3, 5 and 7 after K/BxN serum transfer via intraperitoneal injection of 1 mg of 4-OI. For the hTNFtg arthritis model, 1 mg of 4-OI was administered every third day over a total period of 21 days, starting at 7 weeks of age.

## Histological analysis

Hind paws and long bones of mice were fixed overnight in 4% PFA at 4°C followed by decalcification in 14% EDTA for 14 days until bones were pliable. H&E and TRAP staining via the acid phosphatase leucocyte kit (Sigma-Aldrich) were performed on serial paraffin sections (2  $\mu$ m) of the paw for the quantification of inflammation, bone erosion and osteoclast number. TRAP staining was additionally performed on serial paraffin sections (2  $\mu$ m) of tibial bones for osteoclast detection. Histomorphometric analysis of inflammation area (I.Ar), erosion area (E.Ar), number of osteoclasts per bone perimeter (N.Oc/B.Pm), bone volume per total volume (BV/TV), trabecular thickness (Tb.Th), trabecular number (Tb.N), trabecular space (Tb.Sp) and osteoclast surface per bone surface (Oc.S/BS) was performed using an Axio Lab.A1 microscope (Carl Zeiss), equipped with a digital camera and image analysis system (OsteoMeasure, OsteoMetrics).

## Micro-CT analysis

Long bones were fixed in 4% PFA overnight before the analyses. All micro-CT ( $\mu$ CT) imaging was performed using the cone-beam Desktop Micro Computer Tomograph  $\mu$ CT 40 (SCANCO Medical). The settings were optimised for calcified tissue visualisation at 55 kVp with a current of 145  $\mu$ A and 200 ms integration time for 500 projections per 180° and an isotropic voxel size of 6.0  $\mu$ m. The three-dimensional modelling of the bone was performed with optimised greyscale thresholds of the operating system Open VMS (SCANCO Medical).

## Flow cytometry analysis

Ankles were cut into small pieces with scissors and digested with 1 mg/mL Collagenase A and 0.1 mg/mL DNaseI in RPMI medium (+10% FCS and 1% PS) at 37°C for 1 hour. Digested ankles were put through 40  $\mu$ m cell strainers to obtain a

single-cell suspension. For surface marker staining, cells were first incubated with anti-mouse CD16/32 antibody (Biolegend, clone 93) in 1  $\times$  PBS for 5 min in the dark at 4°C, and then stained with the surface markers: CD45 PerCP Cy5.5 (Biolegend, 30-F11), CD45 EF780 (eBioscience, 30-F11), CD11b BV605 (Biolegend, M1/70), Ly6C PE-Cy7 (Biolegend, HK1.4), CD115 BV421 (Biolegend, AFS98), RANK PE (Biolegend, R12-31) in 1  $\times$  PBS in the dark at 4°C for 20 min. For intracellular staining, cells were washed with 1  $\times$  PBS and incubated in fixation/permeabilisation buffer (Foxp3/Transcription Factor Staining Buffer Set, eBioscience) for 20 min in the dark at room temperature (RT), followed by two washing steps in 1  $\times$  permeabilisation buffer and a 10 min incubation in blocking solution (1  $\times$  permeabilisation buffer + 20% FCS) at RT for 10 min. Cells were then stained with antibodies for the intracellular markers: HIF1 $\alpha$  PE (R&D, IC1935P) or Puromycin Alexa Fluor 488 (Sigma-Aldrich, 12D10) in blocking solution for 1 hour at 4°C in the dark. After washing with 1  $\times$  permeabilisation buffer, cells were resuspended in FACS buffer (1  $\times$  PBS with 2% FCS and 5 mM EDTA) for flow cytometric analyses. Flow cytometry was performed on the Cytotflex S flow cytometer (Beckman Coulter) and data were analysed by Kaluza V.2.1 (Beckman Coulter).

## Single cell energetic metabolism by profiling translation inhibition

Cells isolated from ankle tissue were resuspended in HBSS and stimulated either with 100 mM 2-DG (Sigma-Aldrich) for 10 min at 37°C, with 20  $\mu$ M oligomycin A (Sigma-Aldrich) for 5 min at 37°C or successively with both compounds. All cells were subsequently incubated with 10  $\mu$ g/mL puromycin dihydrochloride (Sigma-Aldrich) in HBSS for 1 hour at 37°C. Cells were then washed in ice-cold 1  $\times$  PBS and stained with antibodies for surface markers, followed by intracellular staining with an anti-puromycin antibody as described in the flow cytometry section.

## Murine osteoclast in vitro differentiation

Total bone marrow cells from mice were isolated by flushing femur and tibia. The cells were plated overnight at 37°C, 5.5% CO<sub>2</sub> in a 100  $\times$  20 mm dish in OC medium ( $\alpha$ MEM + GlutaMax with 10% FCS and 1% PS), containing 5 ng/mL M-CSF (Pepro- tech). The next day, non-adherent bone marrow-derived monocytes (BMMs) were collected, washed and plated at a cell density of 1  $\times$  10<sup>6</sup> cells/mL and 37°C, 5.5% CO<sub>2</sub> in OC medium with 20 ng/mL M-CSF and 10 ng/mL RANKL (Pepro- tech). Medium was exchanged every 2 days. On day 3, when osteoclasts were fully differentiated, cells were washed with PBS, fixed and stained using the acid phosphatase leucocyte kit (Sigma-Aldrich). 4-OI (Cayman Chemical) stimulation occurred on day 1 and 2 of osteoclast cell culture using the concentration indicated in the respective experiment. Stimulation with 0.5 mM N-acetyl-l-cysteine (NAC) (Abcam) was performed on days 1 and 2 of cell culture. Stimulation with 2 mM 2-DG (Sigma-Aldrich) or 5  $\mu$ M cyanide m-chlorophenyl hydrazine (CCCP) (Sigma-Aldrich) was performed on day 1 of cell culture for 3 hours, followed by medium exchange. Stimulation with 20 mM dimethyl-malonate (DMM) (Sigma-Aldrich) was performed on day 1 and 2 of cell culture for 3 hours each day, followed by medium exchange. Images were acquired with the All-in-One Fluorescence Microscope BZ-X710 (KEYENCE) and quantification of osteoclast number was performed with ImageJ.

### Bulk RNA sequencing

Total RNA was extracted on day 3 of osteoclast cell culture and purified with the RNeasy Mini Kit (QIAGEN) according to the manufacturer's instructions. Whole transcriptome RNA sequencing (RNA-seq) was carried out by Novogene (UK) with a total amount of 1 µg RNA per sample. Raw paired-end reads were aligned to the reference genome (mm10) using STAR (V2.5). HTSeq V0.6.1 was used to count the read numbers mapped to each gene. Differential expression analysis between two groups (three biological replicates per group) was performed using the DESeq2 R package.

### Transmission electron microscopy

BMM-derived in vitro differentiated osteoclasts were washed with 1×PBS and fixed with 2.5% glutaraldehyde (Carl Roth) in 0.1 M phosphate buffer for at least 48 hours. Thereupon, cells were post-fixed in 2% buffered osmium tetroxide (Carl Roth) dissolved in 0.1 M phosphate buffer (pH 7.4) for 2 hours and dehydrated in graded alcohol concentrations/propylene oxide and embedded in epoxy resin (Sigma-Aldrich) according to standard protocol. For orientation, 1 µm semithin sections (ultramicrotome, Reichert Ultracut E) were stained with toluidine blue. Ultrathin sections were stained with uranyl acetate and lead citrate and examined with a transmission electron microscope (EM 906E; Carl Zeiss Microscopy). Size and number of mitochondria were determined using ImageJ.

### Extracellular flux analyses with murine cells

$2 \times 10^5$  murine BMMs were plated in Seahorse XF96 Cell Culture Microplates (Agilent Technologies) in a volume of 200 µL and differentiated into osteoclasts as described in the respective section. Extracellular flux assays were performed on days 0–3 of murine in vitro cell culture according to manufacturer's instructions and similarly to the description of the procedure in human cells.

### Immunofluorescence staining

BMMs were plated in 24-well plates containing 12 mm circle cover slips (Thermo Fisher Scientific) at a cell density of  $1 \times 10^6$  cells/mL and cultured under osteoclast differentiating conditions as described above. For detection of mitochondrial reactive oxygen species (ROS), cells were stained with MitoSOX Red (Invitrogen) on days 2 and 3 of cell differentiation, for measurement of mitochondrial membrane potential, cells were stained using the MitoProbe JC-1 Assay Kit (Thermo Fisher Scientific) on day 3 of cell culture and to visualise the F-actin ring formation, cells were stained using the F-Actin Visualisation Biochem Kit (Cytoskeleton) according to the respective manufacturer's protocol. For Hif1α immunofluorescence staining, cells were fixed with 4% PFA, washed with 1×PBS and permeabilised using 0.1% TritonX-100 in 1×PBS. After washing with 1×PBS, cells were incubated with blocking buffer (PBS+1% BSA+0.3 M Glycine+2% goat serum) for 1 hour at RT followed by incubation with the primary antibody solution (HIF1α polyclonal antibody, Cayman Chemical) in blocking buffer at 4°C overnight. After washing, cells were incubated with the secondary antibody solution (goat-anti-rabbit IgG DyLight 650, Invitrogen) and Phalloidin-iFluor 555 (Cytoskeleton) in blocking buffer for 45 min at RT in the dark. After the staining, the circle coverslips were transferred onto microscope slides, mounted with Fluoroshield with DAPI (Sigma-Aldrich) and covered with coverslips. Images were acquired with the All-in-One Fluorescence Microscope BZ-X710 (KEYENCE) for the mitochondrial ROS,

mitochondrial membrane potential and F-Actin staining and using the THUNDER Imager (Leica Microsystems) and the LAS X Software for the Hif1α staining. The generated images were processed using the Imaris (Oxford Instruments) and ImageJ software, respectively.

### Sdh activity assay

BMMs were plated in 24-well plates at a cell density of  $1 \times 10^6$  cells/well in 1 mL and cultured under osteoclast differentiating conditions as described above. On day 3 of cell differentiation, cells were harvested and homogenised using the Sdh Assay Buffer followed by the measurement of Sdh activity via the Succinate Dehydrogenase Activity Colorimetric Assay Kit according to manufacturer's instructions (BioVision).

### CRISPR/Cas9-mediated Hif1a gene editing

Bone marrow cells from murine femur and tibia were plated overnight at 37°C, 5.5% CO<sub>2</sub> in a 100×20 mm dish in OC medium (αMEM+GlutaMAX with 10% FCS and 1% PS), supplemented with 5 ng/mL M-CSF (Peprotech). The next day, non-adherent BMMs were collected and resuspended in primary nucleofection buffer P3 (Lonza) at a concentration of  $1 \times 10^6$  cells/20 µL. The cell suspension was combined with a reaction mixture containing 12.5 µg of Alt-R S.p. Cas9 Nuclease V3 (IDT) and 0.04 nmol pre-designed Alt-R CRISPR-Cas9 single guide RNA for *Hif1a* (Mm.Cas9HIF1A.1AB, IDT) or Alt-R CRISPR-Cas9 Negative Control crRNA (IDT) in a total volume of 5 µL per  $1 \times 10^6$  cells. The mixture was then transferred into cuvettes (P3 primary Cell 4D-Nucleofector X Kit (Lonza)) and nucleofected via the Amaxa 4D Nucleofector (Lonza) using the code CM-137. Immediately after the nucleofection, cells were supplemented with pre-warmed, antibiotic-free αMEM medium and incubated at 37°C for 5 min. The BMMs were then adjusted to a cell density of  $2 \times 10^6$  cells/mL using OC medium with 20 ng/mL M-CSF and 10 ng/mL RANKL (Peprotech) for osteoclast differentiation and plated into 96-well plates at 200 µL/well for TRAP staining and extracellular flux analysis as described in previous sections and into 48-well plates at 500 µL/well for genomic DNA and RNA extraction.

### RNA extraction and real-time PCR for human and murine cells

RNA from in vitro cultivated cells was extracted using RNA-Solv Reagent (VWR Peqlab) according to the manufacturer's instructions. Extracted RNA was freed from genomic DNA using DNase I Kit (Thermo Scientific) and reversely transcribed into cDNA using high capacity cDNA Reverse Transcription Kit (Applied Biosystems). Real-time PCR was performed using Takyon ROX SYBR 2X MasterMix dTTP blue (Eurogentec) on CFX96TM Real-Time System (Bio-Rad) with primers listed in online supplemental tables 1 and 2. Gene expression was normalised against *B2M* for human cells and *Actb1* for murine cells. All primers were purchased from Invitrogen.

### Statistical analysis

All statistical analyses were performed using Graph-Pad Prism Software V.9. Data were presented as mean±SEM. Statistical significance was calculated by two-tailed Student's t-test for two-group comparison and one-way analysis of variance (ANOVA) or two-way ANOVA for multiple comparisons. Statistical details (eg, number of samples/group, number of independent experiments) can be found in the figure legends. P values less than 0.05

were considered statistically significant: \* $p < 0.05$ ; \*\* $p < 0.01$ ; \*\*\* $p < 0.001$ ; \*\*\*\* $p < 0.0001$ .

## RESULTS

### Itaconate suppresses glycolytic activity and in vitro differentiation of osteoclasts from patients with RA

To examine the connection between *Acod1* and RA in human osteoclasts, we collected PBMCs from a group of patients with RA as well as from healthy control donors (HD) and differentiated them into mature osteoclasts. We noticed that the amount of polynucleated TRAP-positive cells, obtained from HD donors was inversely correlated with the mRNA expression level of *ACOD1* in freshly isolated PBMCs before the onset of osteoclast differentiation, supporting the idea that *Acod1* acts as a negative regulator of osteoclast development under healthy conditions (figure 1A). Notably, *ACOD1* mRNA expression was reduced in the PBMCs of patients with active RA as compared with healthy donors while no such downregulation was observed in patients with RA, who were in remission (online supplemental figure 1A). The analysis of itaconate levels in PBMC samples by mass spectrometry revealed no significant difference between healthy donors and active RA patients or RA patients in remission (online supplemental figure 1B). However, itaconate levels were correlated with *ACOD1* mRNA expression (online supplemental figure 1C) and inversely correlated with RA disease activity (online supplemental figure 1D).

We then stimulated PBMCs from RA and healthy donors with the cell-permeable itaconate derivative 4-OI during osteoclast cell culture, observing that RA-derived PBMCs show higher osteoclast differentiation potential than PBMCs from HD controls, as illustrated by increased numbers of polynucleated TRAP-positive cells (figure 1B,C). 4-OI administration, on the other hand, suppressed osteoclast differentiation from RA-derived and HD-derived PBMCs in a dose-dependent manner (figure 1B,C, online supplemental figure 1E,F) and reduced mRNA expression levels of the osteoclast differentiation markers nuclear factor of activated T-cells cytoplasmic 1 (*NFATC1*), TRAP 5 (*ACP5*), matrix metalloproteinase 9 (*MMP9*) and cathepsin K (*CTSK*) (online supplemental figure 1G).

Subsequently, we aimed to evaluate the connection between the antiosteoclastogenic properties of 4-OI and a potential modulation of osteoclast metabolism. We, therefore, performed ATP rate assay analyses with PBMCs from patients with RA and HD controls at different time points throughout osteoclast in vitro differentiation. Here, we discovered that osteoclast development was associated with a gradual shift towards glycolytic ATP production. While osteoclast progenitor cells (day 0) predominantly produced ATP via oxidative phosphorylation (OXPHOS), mature osteoclasts (day 10) derived the majority of their ATP from glycolysis. This metabolic transition occurred earlier and was more pronounced in RA-derived osteoclasts as compared with osteoclasts from HD controls (figure 1D,E). To test the effect of 4-OI on the metabolic profile of developing osteoclasts, we treated the cells with 50  $\mu$ M of 4-OI for 24 hours, followed by glycolytic and mitochondrial stress test assays on day 3 of osteoclast cell culture. RA-derived OCPs showed an increased glycolytic activity and reduced mitochondrial respiration as compared with HD-derived cells in the absence of 4-OI while 4-OI stimulation inhibited glycolytic activity in RA-derived cells (figure 1F–I). Using an ATP rate assay as well as qPCR analysis of the glycolytic genes solute carrier family 2 member 1 (*SLC2A1*), aldolase, fructose-bisphosphate C (*ALDOC*), phosphoglycerate kinase 1 (*PGK1*), enolase 1 (*ENO1*), lactate

dehydrogenase A (*LDHA*) and pyruvate dehydrogenase kinase 1 (*PDK1*), we confirmed the ability of 4-OI to inhibit glycolytic ATP production in HD OCPs (figure 1J,K). Together, our data indicate that RA-associated osteoclasts strongly rely on glycolytic energy production while itaconate suppresses the metabolic shift towards glycolysis in human OCPs and inhibits osteoclast maturation.

### *Acod1*-deficiency exacerbates arthritis and arthritis-associated bone loss in mice

To further analyse the importance of *Acod1* for osteoclast metabolism in the context of inflammatory arthritis, we subjected WT and *Acod1*-deficient mice to the K/BxN serum-induced arthritis model (SIA).<sup>26</sup> *Acod1*<sup>-/-</sup> mice developed stronger inflammation, as illustrated by increased arthritis score, paw swelling and H&E-stained inflammation area (figure 2A–C; online supplemental figure 2A). Along with that, we observed a local increase in osteoclast numbers and bone erosion within the affected joints of *Acod1*<sup>-/-</sup> mice (figure 2A,C) as well as upregulated expression of the osteoclast-associated genes tumour necrosis factor receptor superfamily, member 11 a, NF $\kappa$ B activator (*Tnfrsf11a*), *Nfatc1*, *Acp5*, *Ctsk* and *Mmp9* (online supplemental figure 2B). To find out, if the increase in osteoclast numbers was due to enhanced infiltration by OCPs, we quantified the amount of CD45<sup>+</sup>CD11b<sup>+</sup>Ly6C<sup>hi</sup>CD115<sup>+</sup> cells within the synovial tissue of arthritic WT and *Acod1*<sup>-/-</sup> mice via flow cytometry. While the proportion of OCPs was significantly higher in WT mice with SIA as compared with naïve WT mice, *Acod1*-deficiency did not cause any further changes in OCP number (online supplemental figure 2C,D). However, we discovered that OCPs from the inflamed synovium of *Acod1*<sup>-/-</sup> mice expressed higher levels of receptor activator of NF- $\kappa$ B (Rank) protein than WT OCPs (figure 2D), suggesting that *Acod1* controls inflammatory bone erosion through the regulation of osteoclast differentiation, rather than the recruitment of their progenitors. In order to examine the impact of *Acod1*-deficiency on systemic bone loss in SIA, we performed  $\mu$ CT on tibial bone as well as histomorphometry analyses on TRAP-stained tibial sections. Here, we found that arthritic *Acod1*<sup>-/-</sup> mice are characterised by systemic reduction of bone mass and an increased number of TRAP-positive osteoclasts (figure 2E,F). Naïve *Acod1*<sup>-/-</sup> mice also showed increased osteoclast numbers and osteoclast-covered bone surface when compared with naïve WT mice, despite a lack of difference in bone volume (online supplemental figure 2E,F). These findings demonstrate that *Acod1* inhibits osteoclast development in vivo and protects against both local as well as systemic bone loss in experimental arthritis.

Our human in vitro analyses indicated that mature osteoclasts, derived from the PBMCs of patients with RA, exhibit a greater dependence on glycolysis for ATP production when compared with osteoclasts from healthy donors. In order to investigate, if similar metabolic deviations are present in our experimental arthritis model and whether these changes are linked to *Acod1*, we analysed the metabolic profile of synovial OCPs, obtained from naïve or arthritic WT and *Acod1*<sup>-/-</sup> mice using the SCENITH technique in combination with an antibody panel for OCP surface markers (CD45<sup>+</sup>CD11b<sup>+</sup>Ly6C<sup>hi</sup>CD115<sup>+</sup>).<sup>28</sup> In accordance with our human in vitro data, we discovered that arthritis induction results in increased glycolytic capacity and reduced mitochondrial dependence in WT OCPs. *Acod1*<sup>-/-</sup> OCPs from SIA mice exhibited an even higher level of glycolytic capacity and further reduction of mitochondrial dependence as compared with WT SIA OCPs (figure 2G, online supplemental figure 2G,H). The

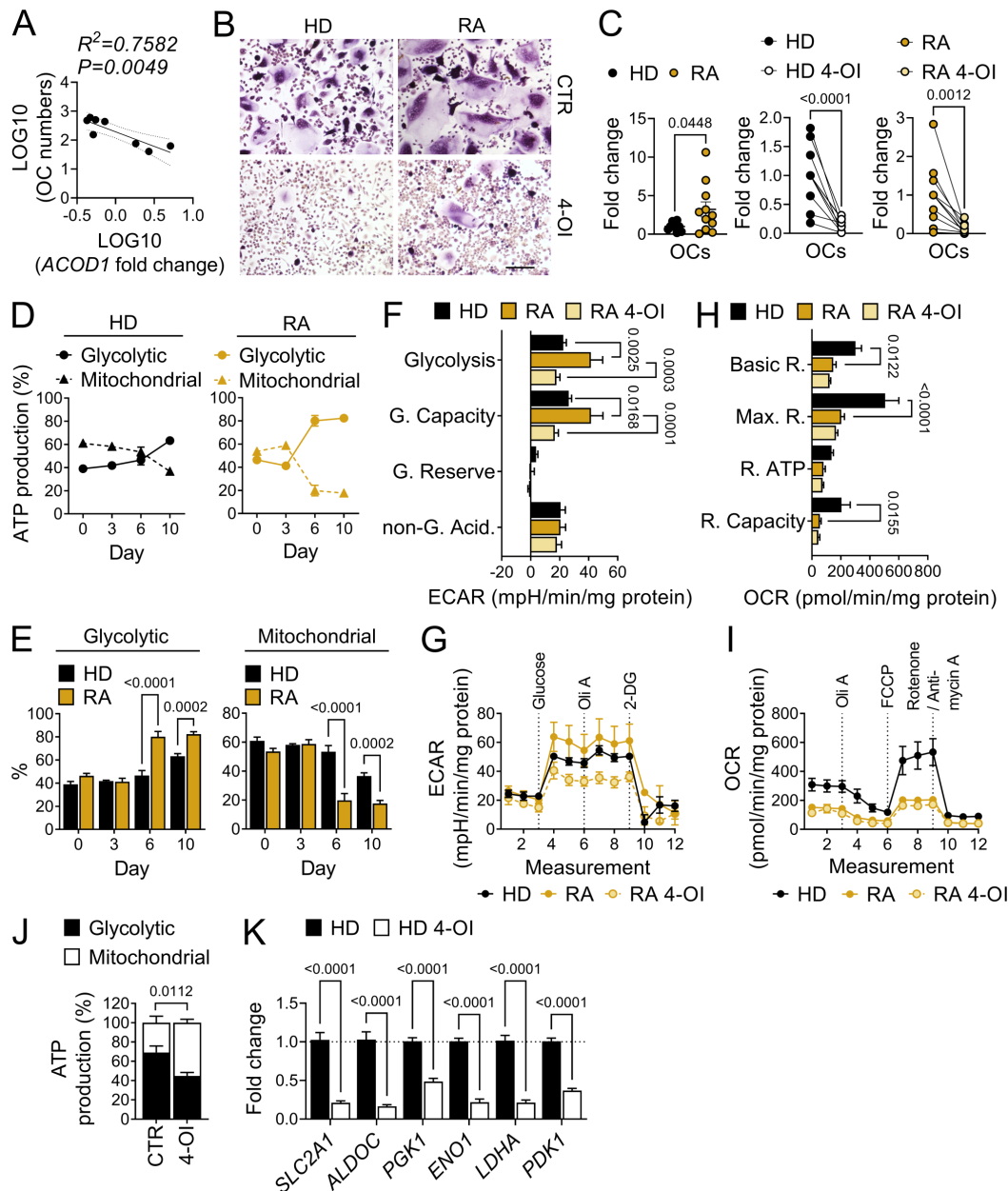


**Figure 1** Itaconate inhibits glycolytic activity and differentiation of human osteoclasts. (A) Correlation analysis between the mRNA expression level of aconitate decarboxylase 1 (*ACOD1*) in peripheral blood mononuclear cells (PBMCs) from healthy donors (HD), measured before the onset of osteoclast in vitro differentiation (day 0), and the numbers of polynucleated osteoclasts ( $\geq 3$  nuclei) from the same donors at the end of osteoclast in vitro differentiation (days 7–10) ( $n=8$ ). (B) Representative pictures and (C) fold change quantification of tartrate-resistant acid phosphatase (TRAP)-positive, polynucleated osteoclasts ( $\geq 3$  nuclei), differentiated from HD or rheumatoid arthritis (RA) patient-derived PBMCs in the presence or absence of  $50 \mu\text{M}$  of 4-octyl-itaconate (4-OI) ( $n=10-11$ ). Scale bar:  $200 \mu\text{m}$ . (D) Percentage of mitochondrial versus glycolytic adenosine triphosphate (ATP) production, determined via ATP rate assay and measured on days 0, 3, 6 and 10 of osteoclast in vitro differentiation in cells derived from HD and RA patients ( $n=4-6$  cell replicates from one RA patient and HD each). (E) Percentage of mitochondrial and glycolytic ATP production in cells derived from HD versus RA patients, determined via ATP rate assay and measured on days 0, 3, 6 and 10 of osteoclast cell culture ( $n=4-6$  cell replicates from one RA patient and one HD). (F) Glycolytic activity parameters and (G) extracellular acidification rate (ECAR) profile plot, determined by glycolytic stress test assay on day 3 of HD and RA patient-derived human osteoclast cell culture after the stimulation with  $50 \mu\text{M}$  4-OI for 24 hours as compared with unstimulated controls (representative of two experiments, each with five cell replicates from one donor per group). (H) Mitochondrial activity parameters and (I) oxygen consumption rate (OCR) profile plot, determined by mitochondrial stress test assay on day 3 of human osteoclast cell culture with HD and RA patient cells after the stimulation with  $50 \mu\text{M}$  4-OI for 24 hours as compared with unstimulated controls (representative of two experiments, each with five cell replicates from one donor per group). (J) Percentage of mitochondrial vs glycolytic ATP production, determined via ATP rate assay on day 3 of human osteoclast in vitro differentiation using HD cells, stimulated with  $50 \mu\text{M}$  4-OI for 24 hours as compared with unstimulated cells (representative of two experiments, each with five cell replicates from one donor). (K) Fold change mRNA expression level of glycolytic genes measured on day 4 of HD osteoclast in vitro differentiation after the stimulation with  $50 \mu\text{M}$  4-OI for 24 hours in comparison to unstimulated cells ( $n=4$  cell replicates). Data are shown as mean  $\pm$  SEM. Symbols represent individual donors. P values were determined by two-tailed Student's t-test for single comparisons and two-way ANOVA for multiple comparisons. Correlations were tested using the linear regression F test. ANOVA, analysis of variance.

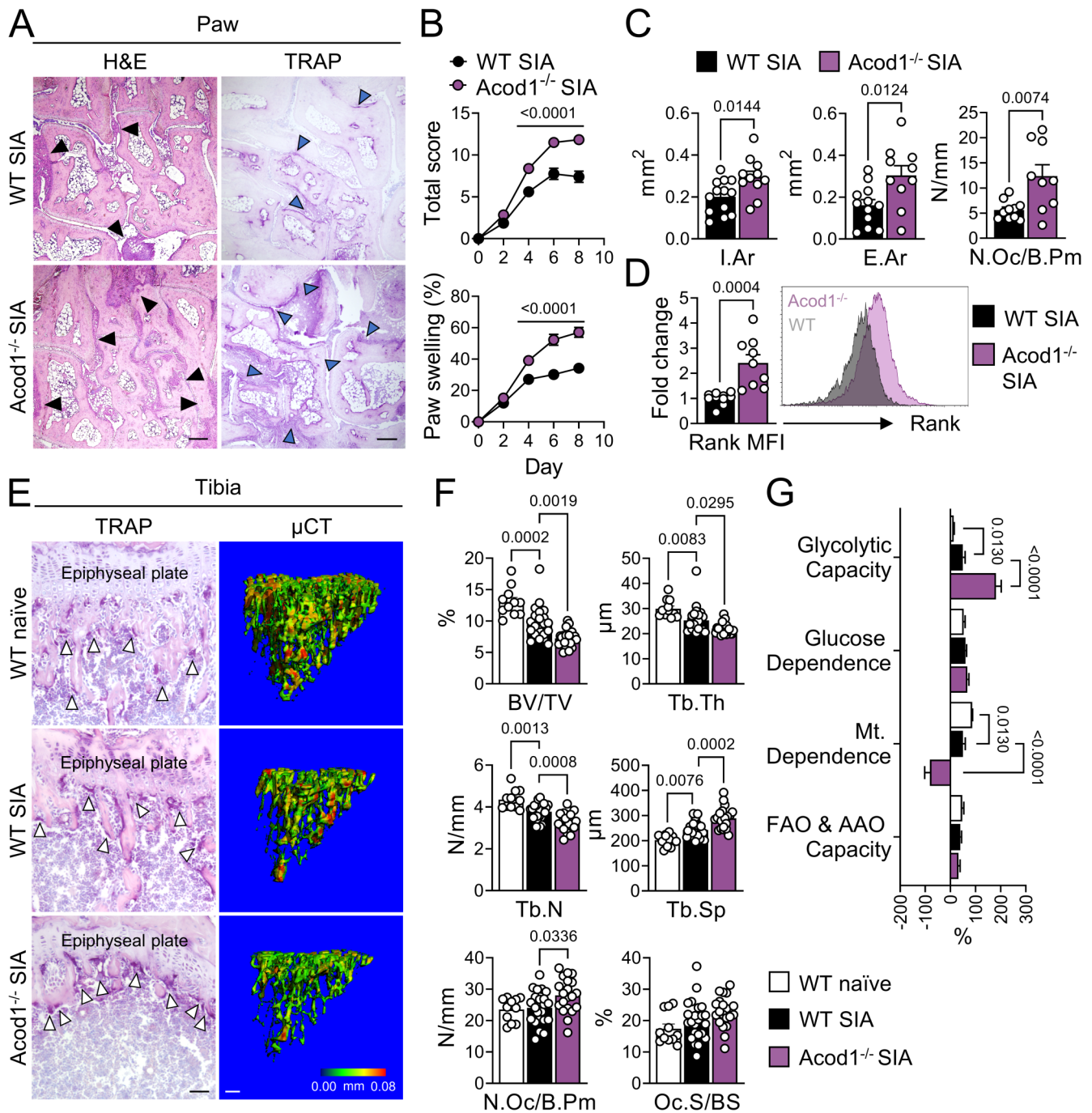


**Figure 2** Acod1-deficiency exacerbates serum-induced arthritis in mice. (A) Representative images of hematoxylin and eosin (H&E) and tartrate-resistant acid phosphatase (TRAP)-stained paw sections from wild-type (WT) and aconitate decarboxylase 1-deficient (Acod1<sup>-/-</sup>) mice with K/BxN serum-induced arthritis (SIA). Black arrowheads (H&E staining) indicate inflammation, blue arrowheads (TRAP staining) indicate eroded bone tissue with osteoclasts. Scale bar: 200 μm. (B) Arthritis score and proportional paw swelling in WT and Acod1<sup>-/-</sup> mice during the course of SIA (n=21–23). (C) Quantification of inflammation area (I.Ar), eroded bone area (E.Ar) and osteoclast number per bone perimeter (N.Oc/B.Pm) in H&E and TRAP-stained paw tissue sections of WT and Acod1<sup>-/-</sup> mice with SIA (n=9–13). (D) Flow cytometry analysis of receptor activator of NF-κB (Rank) expression in CD45<sup>+</sup>CD11b<sup>+</sup>Ly6C<sup>hi</sup>CD115<sup>+</sup> osteoclast precursors (OCPs) in the synovial ankle tissue of WT and Acod1<sup>-/-</sup> mice with SIA, depicted as fold changes of the mean fluorescence intensity (MFI) in Acod1<sup>-/-</sup> as compared with WT cells (n=9–10). (E) Representative images of TRAP staining and micro-CT (μCT) analysis of tibiae from naïve and SIA affected WT as well as SIA affected Acod1<sup>-/-</sup> mice. White arrowheads indicate osteoclasts. Scale bar TRAP: 50 μm. Scale bar μCT: 200 μm. (F) Quantification of bone volume per total volume (BV/TV), trabecular thickness (Tb.Th), trabecular number (Tb.N), trabecular space (Tb.Sp), number of osteoclasts per bone perimeter (N.Oc/B.Pm) and osteoclast surface per bone surface (Oc.S/BS) (n=11–23). (G) SCENITH analysis of metabolic parameters in OCPs from WT mice with and without SIA and Acod1<sup>-/-</sup> mice with SIA (n=4–5). Data are shown as mean±SEM. Symbols represent individual mice. P values were determined by two-tailed Student's t-test for single comparisons and one-way or two-way ANOVA for multiple comparisons. ANOVA, analysis of variance.

levels of glucose dependence as well as the capacity for fatty acid and amino acid oxidation (FAO and AAO) on the other hand remained mostly similar in WT naïve, WT SIA and *Acod1*<sup>-/-</sup> SIA OCPs, indicating that arthritis induction and *Acod1*-deficiency have little influence on the preferred energy source that is used for ATP generation in synovial OCPs (figure 2G). Our results, therefore, suggest that SIA causes a metabolic reprogramming of OCPs towards glycolytic ATP production while *Acod1* acts as a negative regulator of this process.

### Acod1-dependent suppression of osteoclast differentiation is accompanied by an alteration of the osteoclast transcriptional network

To delineate the mechanism behind the influence of *Acod1* on osteoclast development and metabolic activity, we performed osteoclast in vitro differentiation assays with BMMs, isolated from WT and *Acod1*<sup>-/-</sup> mice. *Acod1*-deficiency resulted in enhanced osteoclast differentiation, as demonstrated by the elevated number of TRAP-positive polynucleated cells, increased actin-ring formation as well as an upregulated mRNA expression of osteoclast-related genes (figure 3A–C, online supplemental figure 3A). We presumed that the cellular phenotype of *Acod1*<sup>-/-</sup> osteoclasts is caused by itaconate-deficiency (online supplemental figure 3B). In accordance, the addition of 4-OI to the cell culture abolished the pro-osteoclastogenic effect of *Acod1*-deficiency and inhibited the ability of WT BMMs to differentiate into mature osteoclasts in a dose-dependent manner, without affecting cell viability (figure 3A–C, online supplemental figure 3C–F). Furthermore, through mass spectrometry analysis, we detected 4-OI within the cell lysates of 4-OI stimulated osteoclasts, thus confirming its capacity to enter the cells (online supplemental figure 3G).

To ascertain the influence of the *Acod1*-itaconate axis on the genomic transcriptional network of osteoclasts, we performed a whole transcriptome RNAseq analysis with fully differentiated osteoclasts from WT and *Acod1*-deficient mice that were cultured in the presence or absence of 100 µM 4-OI. A principal component analysis (PCA) showed that samples from unstimulated WT osteoclasts (WT), unstimulated *Acod1*-deficient osteoclasts (*Acod1*<sup>-/-</sup>) and 4-OI stimulated *Acod1*-deficient osteoclasts (*Acod1*<sup>-/-</sup> 4-OI) were grouped in separate clusters, indicating that *Acod1*-deficiency and 4-OI stimulation result in a clear change of the transcriptional profile (online supplemental figure 3H). In particular, 1279 genes were differentially expressed in *Acod1*-deficient as compared with WT osteoclasts while 4-OI stimulation of *Acod1*<sup>-/-</sup> osteoclasts changed the expression of 6022 genes (online supplemental figure 3I). Among the 1279 genes that were affected by *Acod1*-deficiency in the absence of 4-OI, 800 genes (62.55%) were also changed in 4-OI stimulated *Acod1*<sup>-/-</sup> as compared with unstimulated *Acod1*<sup>-/-</sup> osteoclasts (figure 3D). In line with the hypothesis that *Acod1* suppresses osteoclast differentiation by modulating their metabolic state, a gene ontology (GO) over-representation analysis (ORA) identified significant enrichment of several metabolic pathways among the genes that were affected by the presence of *Acod1* and 4-OI. These pathways include the NADH metabolic process, cellular respiration and responses to hypoxia and ROS (figure 3E). Using gene set enrichment analyses, we furthermore demonstrated that aside from the osteoclast differentiation pathway, pathways related to ROS, hypoxia and RA were significantly upregulated in *Acod1*<sup>-/-</sup> as compared with WT osteoclasts (figure 3F, online supplemental figure 3J). A heatmap analysis of the genes that were mapped to the osteoclast differentiation

pathway as well as to the response to hypoxia and ROS pathways showed that *Acod1*-deficiency and 4-OI stimulation regulate the expression of these genes in opposite directions. This supports the notion that the effect of *Acod1*-deficiency on the transcriptional network of osteoclasts can mostly be attributed to a lack of itaconate and can be reversed through supplementation with an itaconate derivative (figure 3G).

### Acod1 suppresses Hif1 $\alpha$ -mediated induction of aerobic glycolysis

As a next step, we performed a time course analysis of glycolytic and mitochondrial activity throughout the osteoclastogenesis using extracellular flux assays. Consistently with our human in vitro data, we observed that WT osteoclast differentiation is associated with progressive reduction of OXPHOS and a simultaneous increase in glycolytic activity, emphasising the importance of a glycolytic switch during osteoclast maturation (figure 4A). As expected, we furthermore discovered that the enhanced osteoclast differentiation potential in the absence of *Acod1* is linked to metabolic reprogramming. Thus, mature *Acod1*-deficient osteoclasts are characterised by reduced mitochondrial respiration as well as enhanced glycolytic activity and elevated mRNA expression of glycolytic enzymes. *Acod1*<sup>-/-</sup> osteoclasts are accordingly more dependent on glycolytic ATP production than WT osteoclasts (figure 4B–F, online supplemental figure 4A), supporting the notion that *Acod1* counteracts the glycolytic shift accompanying osteoclast maturation.

To examine, if metabolic reprogramming could be responsible for *Acod1*-dependent changes in osteoclast differentiation, we incubated WT BMMs with 5 µM of CCCP and WT and *Acod1*<sup>-/-</sup> BMMs with 2 mM of 2-DG for 3 hours at the beginning of osteoclast in vitro cell culture. The chemical uncoupler CCCP reduces the electrochemical proton gradient, thereby suppressing OXPHOS-mediated ATP production while 2-DG suppresses glycolytic ATP production through competitive inhibition of glucose transport as well as the conversion of glucose into glucose-6-phosphate.<sup>29–30</sup> In accordance with the observation that osteoclast differentiation is associated with enhanced glycolytic activity and reduced OXPHOS, we detected an increased number of polynucleated TRAP-positive osteoclasts in response to stimulation with CCCP while the glycolytic inhibitor 2-DG strongly suppressed the ability of WT and *Acod1*<sup>-/-</sup> BMMs to differentiate into osteoclasts, without affecting their viability (online supplemental figure 4B–G).

One of the most important regulators of metabolic reprogramming is the transcription factor hypoxia-inducible factor 1 (Hif1). Hif proteins consist of a constitutively expressed  $\beta$  subunit (Hif1 $\beta$ / Aryl hydrocarbon receptor nuclear translocator (Arnt)) and an oxygen-dependent  $\alpha$  subunit (Hif1 $\alpha$ , Hif2 $\alpha$  or Hif3 $\alpha$ ). However, of the three  $\alpha$  subunit homologues, Hif1 $\alpha$  is the one that is required for the regulation of glycolytic gene expression.<sup>31</sup> As itaconate was previously shown to limit Hif1 $\alpha$  activity,<sup>20</sup> we aimed to determine, if the osteoclast phenotype of *Acod1*-deficient mice is linked to changes in Hif1 $\alpha$  protein expression. We, therefore, first measured the amount of Hif1 $\alpha$  protein over the course of WT osteoclast in vitro differentiation using the Meso Scale Discovery (MSD) kit. In the presence of sufficient oxygen levels, Hif1 $\alpha$  normally undergoes prolyl hydroxylase domain (Phd)-mediated hydroxylation, followed by von Hippel-Lindau (Vhl) protein binding and subsequent proteasomal degradation.<sup>32–34</sup> In order to mimic hypoxic conditions for Hif1 $\alpha$  stabilisation, we incubated the differentiating osteoclasts with cobalt chloride (CoCl<sub>2</sub>), which prevents the



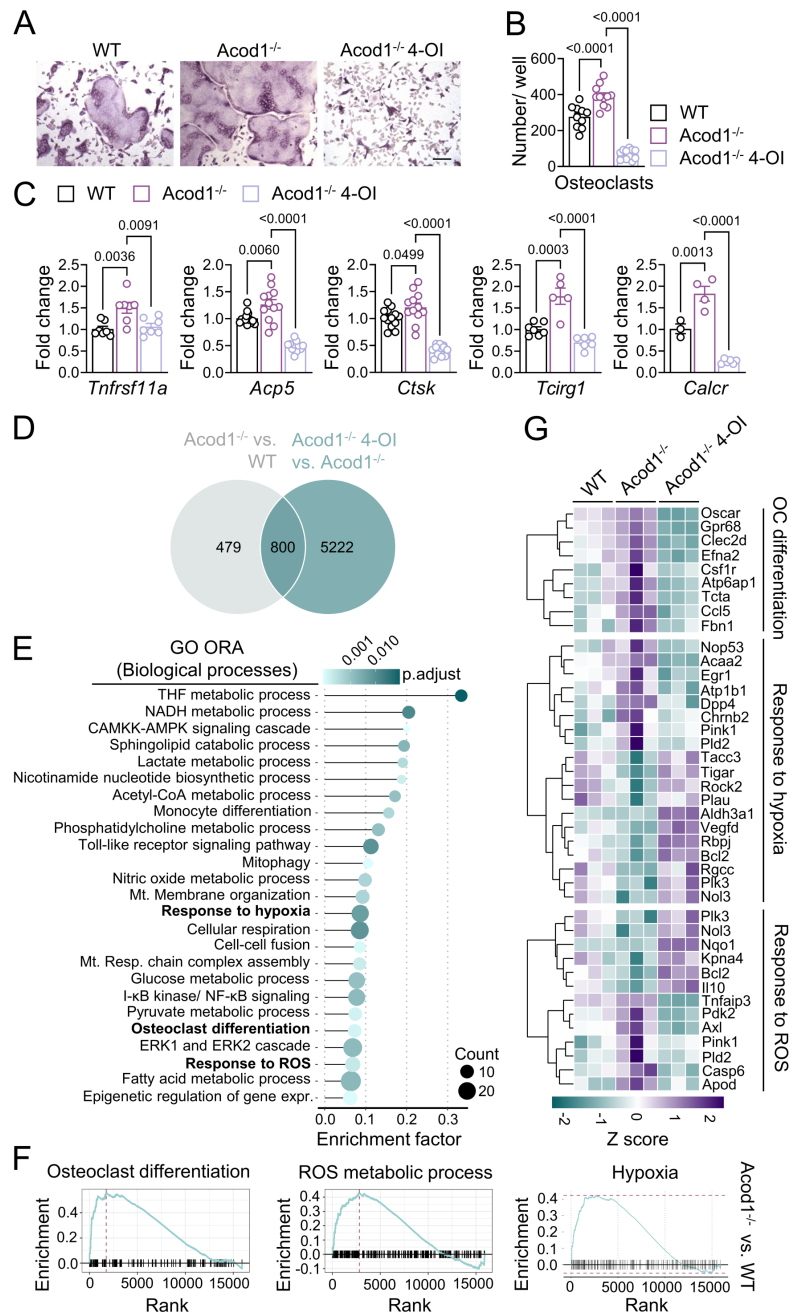


**Figure 3** *Acod1*-deficiency alters metabolic gene expression and enhances murine osteoclastogenesis. (A) Representative images and (B) quantification of tartrate-resistant acid phosphatase (TRAP)-stained polynucleated ( $\geq 5$  nuclei) osteoclasts that were differentiated from bone marrow monocytes of wild-type (WT) and aconitate decarboxylase 1-deficient (*Acod1*<sup>-/-</sup>) mice that were either unstimulated or stimulated with 100  $\mu$ M 4-octyl-itaconate (4-OI) for 48 hours ( $n=10-11$ ). Scale bar: 100  $\mu$ m. (C) Fold change expression levels of osteoclast-related genes in *Acod1*<sup>-/-</sup> osteoclasts (day 3 of cell culture) that were either unstimulated or stimulated with 100  $\mu$ M 4-OI for 48 hours as compared with unstimulated WT osteoclasts ( $n=3-13$ ). (D) Venn diagram of differentially expressed genes in unstimulated *Acod1*<sup>-/-</sup> osteoclasts as compared with unstimulated WT osteoclasts (*Acod1*<sup>-/-</sup> vs WT) and in 4-OI stimulated *Acod1*<sup>-/-</sup> osteoclasts as compared with unstimulated *Acod1*<sup>-/-</sup> osteoclasts (*Acod1*<sup>-/-</sup> 4-OI vs *Acod1*<sup>-/-</sup>) following an RNA sequencing and differential gene expression analysis using the DESeq2 method with a p value cut-off of 0.05. (E) Overrepresentation analysis (ORA) of gene ontology (GO) biological processes using the overlapping set of genes that were differentially expressed in the comparison *Acod1*<sup>-/-</sup> vs WT as well as in the comparison *Acod1*<sup>-/-</sup> 4-OI vs *Acod1*<sup>-/-</sup>. The graph shows a lollipop chart of overrepresented GO terms with a p value cut-off of 0.05. The position on the x-axis gives the enrichment factor and the dot size gives the number of genes present in each ontology. A list of the enriched pathways with their related genes for the GO ORA analysis is attached as online supplemental file 2 (ard-2023-224774\_RNA-Seq\_Enriched pathways). (F) Gene set enrichment analysis (GSEA) for GO and Kyoto Encyclopaedia of Genes and Genomes (KEGG) enrichment in *Acod1*<sup>-/-</sup> osteoclasts as compared with WT osteoclasts with a p value cut-off of 0.05 and visualisation of the hallmark terms 'osteoclast differentiation', 'hypoxia' and 'reactive oxygen species (ROS) metabolic process'. (G) Heatmap illustrating the H-clusters of differentially expressed genes that were assigned to the GO terms 'osteoclast differentiation', 'response to hypoxia' and 'response to ROS' within the groups WT, *Acod1*<sup>-/-</sup> and *Acod1*<sup>-/-</sup> 4-OI. A gene list with the corresponding fold change data and statistical values is attached as online supplemental file 3 (ard-2023-224774\_RNA-Seq\_Heatmap\_Genelist). Data are shown as mean  $\pm$  SEM. Symbols represent individual mice. P values were determined by one-way ANOVA for multiple comparisons. ANOVA, analysis of variance.

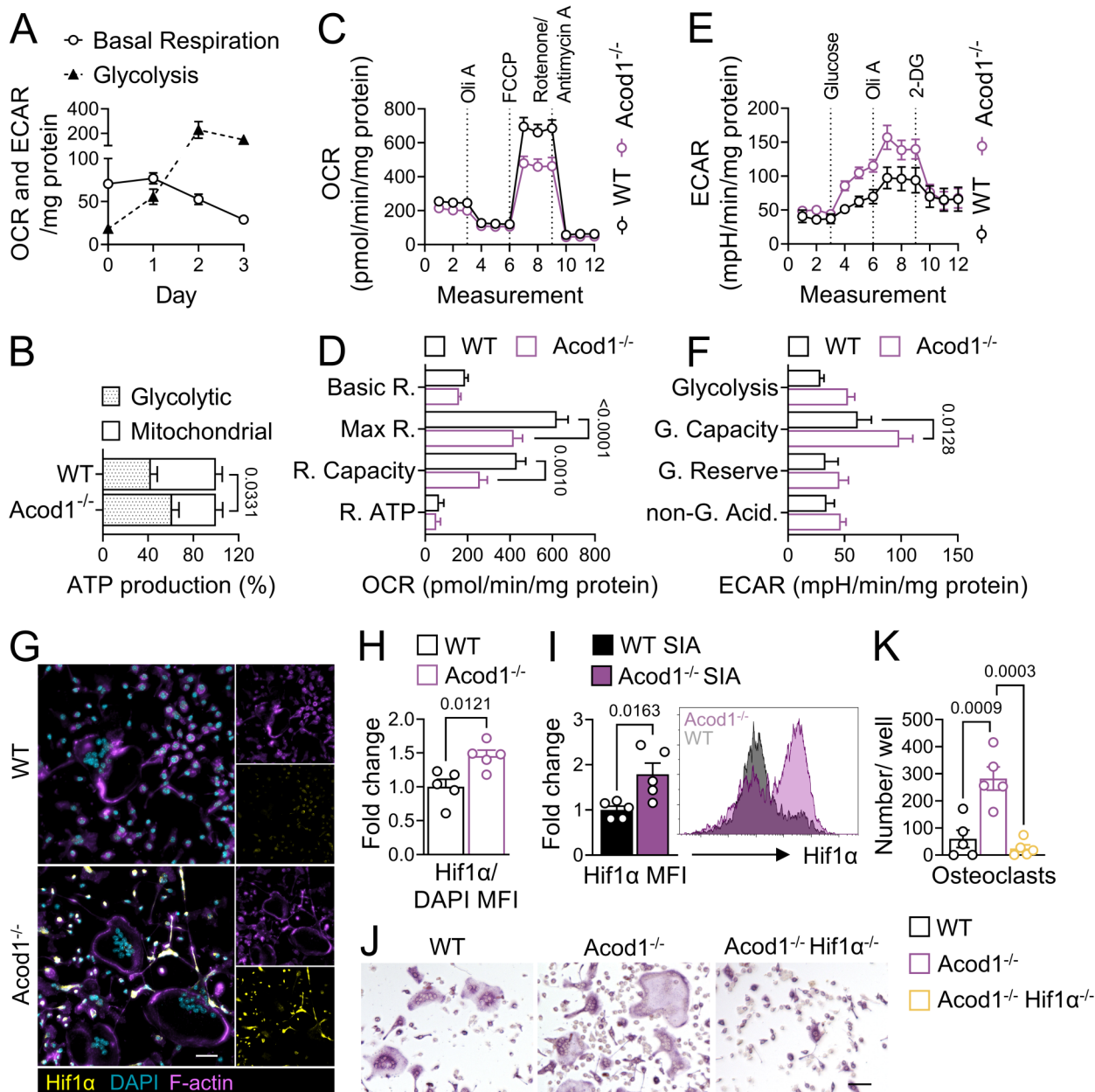


**Figure 4** Acod1-deficiency promotes switch towards glycolysis in a Hif1 $\alpha$ -dependent manner. (A) Time course analysis of glycolytic and mitochondrial activity in wild-type (WT) cells throughout osteoclast differentiation, determined by mitochondrial and glycolytic stress test assays on days 0, 1, 2 and 3 of osteoclast cell culture and quantification of oxygen consumption rate (OCR) and extracellular acidification rate (ECAR) as a measure for basal respiration and glycolysis, respectively (n=6–13). (B) Quantification of the percentage of glycolytic versus mitochondrial adenosine triphosphate (ATP) production in osteoclasts (day 3 of cell culture) from WT and aconitate decarboxylase 1-deficient (Acod1<sup>-/-</sup>) mice, determined by ATP rate assay (n=12–15). (C) OCR profile plot and (D) mitochondrial function parameters in osteoclasts (day 3 of cell culture) from WT and Acod1<sup>-/-</sup> mice, determined by mitochondrial stress test assay (n=25–29). (E) ECAR profile plot and (F) glycolytic activity parameters in WT and Acod1<sup>-/-</sup> osteoclasts (day 3 of cell culture), determined by glycolytic stress test assay (n=12–16). (G) Representative images of immunofluorescent staining for hypoxia-inducible factor (Hif)-1 $\alpha$  (yellow), F-actin (purple) and DAPI (blue) and (H) fold change quantification of the Hif1 $\alpha$ /DAPI mean fluorescence intensity (MFI) in osteoclasts (day 3 of cell culture) from Acod1<sup>-/-</sup> as compared with WT mice (n=5). Scale bar: 50  $\mu$ m. (I) Flow cytometry analysis of Hif1 $\alpha$  expression in CD45<sup>+</sup>CD11b<sup>+</sup>Ly6C<sup>hi</sup>CD115<sup>+</sup> osteoclast precursors (OCPs) in the synovial ankle tissue of WT and Acod1<sup>-/-</sup> mice with serum-induced arthritis (SIA), depicted as fold changes of the MFI in Acod1<sup>-/-</sup> as compared with WT cells (n=5). (J) Representative images and (K) quantification of tartrate-resistant acid phosphatase (TRAP)-stained polynucleated osteoclasts ( $\geq 5$  nuclei) from Acod1<sup>-/-</sup> mice that were subjected to CRISPR/Cas9-mediated deletion of *Hif1a* gene or from WT and Acod1<sup>-/-</sup> mice that were treated with a non-targeting control construct on day 0 of osteoclast cell culture (n=5). Scale bar: 100  $\mu$ m. Data are shown as mean $\pm$ SEM. Symbols represent individual mice. P values were determined by two-tailed Student's t-test for single comparisons and one-way ANOVA or two-way ANOVA for multiple comparisons. ANOVA, analysis of variance.

hydroxylation and thus degradation of Hif1 $\alpha$  by binding to the Phd iron-binding domain.<sup>35</sup> We generally observed an increased Hif1 $\alpha$  protein expression on day 3 as compared with days 1

and 2 of WT osteoclast cell culture. Although CoCl<sub>2</sub>-stimulated cells exhibited overall increased Hif1 $\alpha$  protein levels, Hif1 $\alpha$  was also upregulated in mature osteoclasts in the absence of CoCl<sub>2</sub>,

indicating that osteoclast differentiation is associated with Hif1 $\alpha$  stabilisation even under normoxic conditions (online supplemental figure 4H). Next, we performed immunofluorescent staining of Hif1 $\alpha$  protein in mature, in vitro differentiated WT and Acod1<sup>-/-</sup> osteoclasts. Here, we observed increased levels of Hif1 $\alpha$  protein in the absence of Acod1 (figure 4G,H). Interestingly, the strongest Hif1 $\alpha$  immunofluorescence signal was not detected within the largest multinucleated osteoclasts, but rather in mononucleated and polynucleated cells that were characterised by pronounced actin-rich membrane protrusions extending to neighbouring cells. This might indicate that Hif1 $\alpha$  is involved in osteoclast-associated cell fusion.<sup>36</sup> Furthermore, we detected increased Hif1 $\alpha$  protein expression in synovial OCPs from Acod1-deficient mice as compared with WT SIA mice via flow cytometry analysis (figure 4I). These data imply that Acod1 may modulate the metabolic state and differentiation of osteoclasts by downregulating Hif1 $\alpha$  protein levels. To evaluate the significance of Hif1 $\alpha$  for the Acod1-dependent regulation of osteoclast differentiation and metabolism, we performed CRISPR/Cas9-mediated knockout of *Hif1a* in Acod1-deficient BMMs. *Hif1a* depletion prevented both the upregulation of osteoclast differentiation and the enhancement of glycolytic activity in the absence of Acod1, as determined by TRAP staining and a glycolytic stress test assay (figure 4J,K, online supplemental figure 4I,J), allowing the conclusion that Acod1 suppresses osteoclast differentiation by inhibiting the Hif1 $\alpha$ -mediated induction of aerobic glycolysis.

#### Acod1 inhibits mitochondrial fission, membrane hyperpolarisation and Sdh-mediated ROS production

To further define the role of Acod1 in osteoclast metabolism, we aimed to analyse the functional state of mitochondria, which is often reflected in their morphology. Using transmission electron microscopy imaging, we discovered that Acod1-deficient osteoclasts, which show reduced mitochondrial respiration as compared with WT osteoclasts, also contain smaller mitochondria. As expected, this reduction in mitochondrial size was prevented in Acod1<sup>-/-</sup> osteoclasts that were cultured in the presence of 4-OI (figure 5A,B). Moreover, Acod1-deficiency led to increased mRNA expression of the fission factor dynamin-1-like protein (Drp1, encoded by the gene *Dnm1l*), which was mitigated by subsequent 4-OI supplementation, suggesting an inhibitory role for Acod1 and itaconate in mitochondrial fission (figure 5C). Mitochondrial fragmentation is linked to physiological cell features, such as increased generation of ROS and changes of the mitochondrial membrane potential.<sup>37</sup> To analyse the impact of Acod1 on ROS production in osteoclasts, we performed MitoSOX immunofluorescent staining at different time points of osteoclast in vitro differentiation. Here, we found that Acod1-deficiency increased ROS production on day 2 of osteoclast development, although we did not detect a significant ROS level difference in mature osteoclast from Acod1<sup>-/-</sup> mice as compared with WT mice (figure 5D,E). To evaluate the mechanistic involvement of ROS in Acod1-mediated regulation of osteoclast development, we treated WT and Acod1<sup>-/-</sup> BMMs with the ROS-scavenger NAC during osteoclast differentiation.<sup>38</sup> Treatment with NAC diminished osteoclast formation irrespective of Acod1 presence and attenuated the upregulation of Hif1 $\alpha$  in Acod1-deficient cells (online supplemental figure 5A–D), implying that the capacity of Acod1 to suppress Hif1 $\alpha$  protein levels and osteoclast maturation is linked to a reduction in ROS formation.

Itaconate was previously shown to modulate the catalytic activity of Sdh—a mitochondrial enzyme complex that catalyses

the oxidation of succinate to generate fumarate.<sup>39</sup> Since this reaction is associated with ROS production as well as Hif1 $\alpha$  stabilisation, we aimed to determine, if a modification of Sdh activity might be involved in Acod1-mediated regulation of osteoclast metabolism.<sup>40</sup> Indeed, we observed enhanced Sdh activity in Acod1<sup>-/-</sup> compared with WT osteoclasts while the inhibition of Sdh using DMM abolished the pro-osteoclastogenic effect of Acod1-deficiency and reduced Hif1 $\alpha$  protein levels in Acod1<sup>-/-</sup> osteoclasts (figure 5F, online supplemental figure 5A–D).

Finally, we also analysed the mitochondrial membrane potential in osteoclasts using the dual-emission potentiometric dye JC-1. Acod1<sup>-/-</sup> osteoclasts showed a higher proportion of red-labelled versus green-labelled mitochondria as compared with WT osteoclasts, indicating that Acod1 promotes mitochondrial membrane depolarisation (figure 5G,H). In summary, our findings suggest that the inhibitory effect of Acod1 on osteoclast differentiation is associated with reduced mitochondrial fragmentation and mitochondrial membrane potential and involves the suppression of Sdh activity, which results in decreased ROS production and subsequent downregulation of Hif1 $\alpha$ -dependent glycolytic metabolism.

#### Therapeutic treatment with 4-OI mitigates inflammation and inflammatory bone loss in experimental arthritis

Acod1-deficiency promotes osteoclast development in vivo and in vitro, suggesting that Acod1 and its enzymatic product itaconate might exhibit a protective effect against arthritis-related bone loss. We, therefore, tested the therapeutic function of the itaconate-derivative 4-OI in SIA. For that purpose, we administered 1 mg of 4-OI on days 1, 3, 5 and 7 after arthritis induction (online supplemental figure 6A). Indeed, we observed an overall reduction of arthritis score, paw swelling and inflamed tissue area as well as decreased osteoclast numbers and local bone erosion within the affected joints, in response to 4-OI treatment (figure 6A–C). We could not detect any difference regarding the number of CD45<sup>+</sup>CD11b<sup>+</sup>Ly6C<sup>hi</sup>CD115<sup>+</sup> OCPs within the synovial tissue of 4-OI treated mice as compared with untreated mice (online supplemental figure 6B). However, we found that the synovial OCPs from 4-OI treated mice exhibited reduced Rank protein levels in comparison to control mice (figure 6D), which is in line with our previous observation that Acod1-deficiency does not affect OCP mobilisation but enhances Rank expression. Quantification of TRAP-positive cells in tibial sections revealed that 4-OI treatment diminished the number of osteoclasts in arthritic mice not only locally, within the affected joints, but also systemically. This, however, was not reflected in reduced systemic bone loss (figure 6E,F).

Since our data indicate that the influence of Acod1 and itaconate on osteoclasts is mediated by metabolic reprogramming, we analysed the effect of 4-OI treatment on the metabolic state of synovial OCPs using SCENITH. Here, we confirmed that experimental arthritis is associated with a transition in OCP metabolism towards glycolysis, as illustrated by strongly increased glycolytic capacity and reduced mitochondrial dependence in K/BxN serum injected mice in comparison to naïve mice (figure 6G, online supplemental figure 6C). On the other hand, 4-OI administration restored the mitochondrial dependence and reduced the glycolytic capacity of OCPs from arthritic mice, thereby reversing the metabolic switch towards glycolysis (figure 6G, online supplemental figure 6C). Interestingly, 4-OI treatment also resulted in increased fatty acid and amino acid oxidation and reduced glucose dependence in synovial OCPs from arthritic mice, meaning that in contrast to Acod1-deficiency,

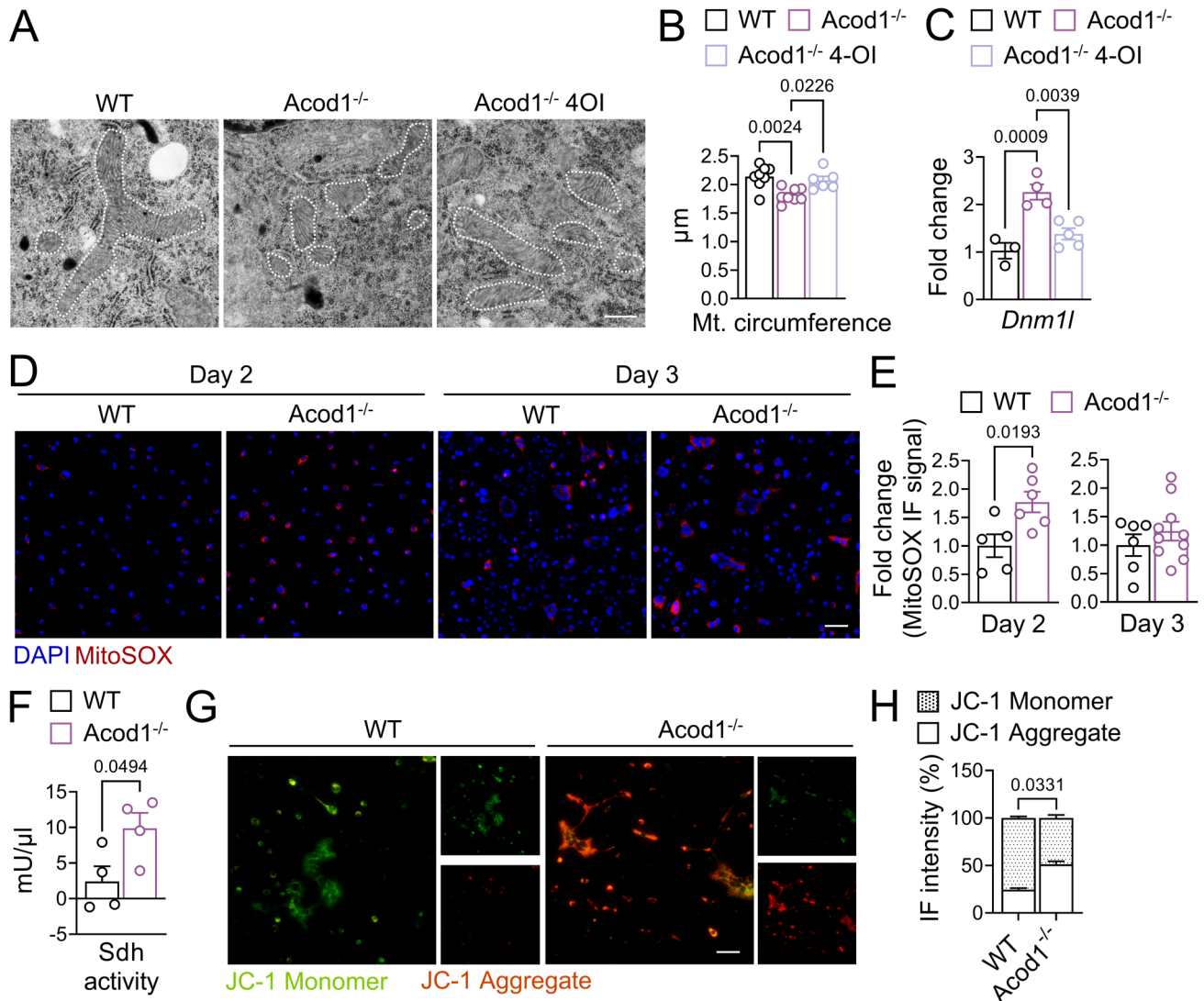


**Figure 5** Acod1-deficiency promotes mitochondrial fission, reactive oxygen species (ROS) formation and membrane hyperpolarisation. (A) Representative transmission electron microscopy (TEM) images and (B) measurement of mitochondrial circumference in wild-type (WT) and aconitate decarboxylase 1-deficient (Acod1<sup>-/-</sup>) osteoclasts (day 3 of cell culture) that were either unstimulated or stimulated with 100 µM 4-octyl-itaconate (4-OI) for 48 hours (n=6–8 individual osteoclasts from 3 mice in each group, symbols represent individual osteoclasts). Representative mitochondria are outlined by white dashed lines. Scale bar: 0.5 µm. (C) mRNA expression analysis of the fission marker gene dynamin 1-like (*Dnm11*) in WT and Acod1<sup>-/-</sup> osteoclasts (day 3 of cell culture) that were either unstimulated or stimulated with 100 µM 4-OI for 48 hours (n=3–5). (D) Representative images and (E) fold change quantification of immunofluorescence (IF) staining for MitoSOX (red) and DAPI (blue) in Acod1<sup>-/-</sup> as compared with WT cells on days 2 and 3 of osteoclast cell culture (n=5–6). Scale bar: 100 µm. (F) Quantification of succinate dehydrogenase (Sdh) activity in WT and Acod1<sup>-/-</sup> osteoclasts (day 3 of cell culture) (n=4). (G–H) Analysis of mitochondrial membrane potential in WT and Acod1<sup>-/-</sup> osteoclasts (day 3 of cell culture) using IF microscopy staining for JC-1. (G) Representative images for JC-1 IF staining. JC-1 monomers are depicted in green and JC-1 aggregates are shown in red. Scale bar: 100 µm. (H) Quantification of the ratio between JC-1 monomers and JC-1 aggregates (n=9–12). Data are shown as mean±SEM. Symbols represent individual mice unless stated otherwise. P values were determined by two-tailed Student's t-test for single comparisons and one-way ANOVA for multiple comparisons. ANOVA, analysis of variance.

4-OI treatment also changed the preferred source for ATP generation (figure 6G, online supplemental figure 6C). Consistently with the ability of 4-OI to downregulate glycolytic capacity, we also observed reduced Hif1α protein expression in OCPs from 4-OI treated arthritis mice using flow cytometry analysis (figure 6H).

To ensure that the uncovered role of itaconate in arthritis-associated bone loss is not limited to the acute K/BxN SIA model, we also tested the therapeutic potential of 4-OI in transgenic mice that express human TNFα (hTNFtg) and spontaneously develop an erosive and chronic inflammatory arthritis<sup>25</sup> (online supplemental figure 7A). The treatment led to an overall alleviation of

the disease phenotype, notably reducing the arthritis score, paw and ankle swelling, inflammation and bone erosion within the joints as well as the osteoclast counts in the tibial bone (online supplemental figure 7B–H). In alignment with the K/BxN SIA model, we also observed that while the percentage of synovial OCPs remained unchanged after 4-OI treatment, Hif1α protein expression was decreased in these cells (online supplemental figure 7I–K). In conclusion, our results confirm that the therapeutic use of 4-OI can limit the glycolytic shift in OCPs, resulting in a mitigation of inflammation-associated bone loss in experimental arthritis.

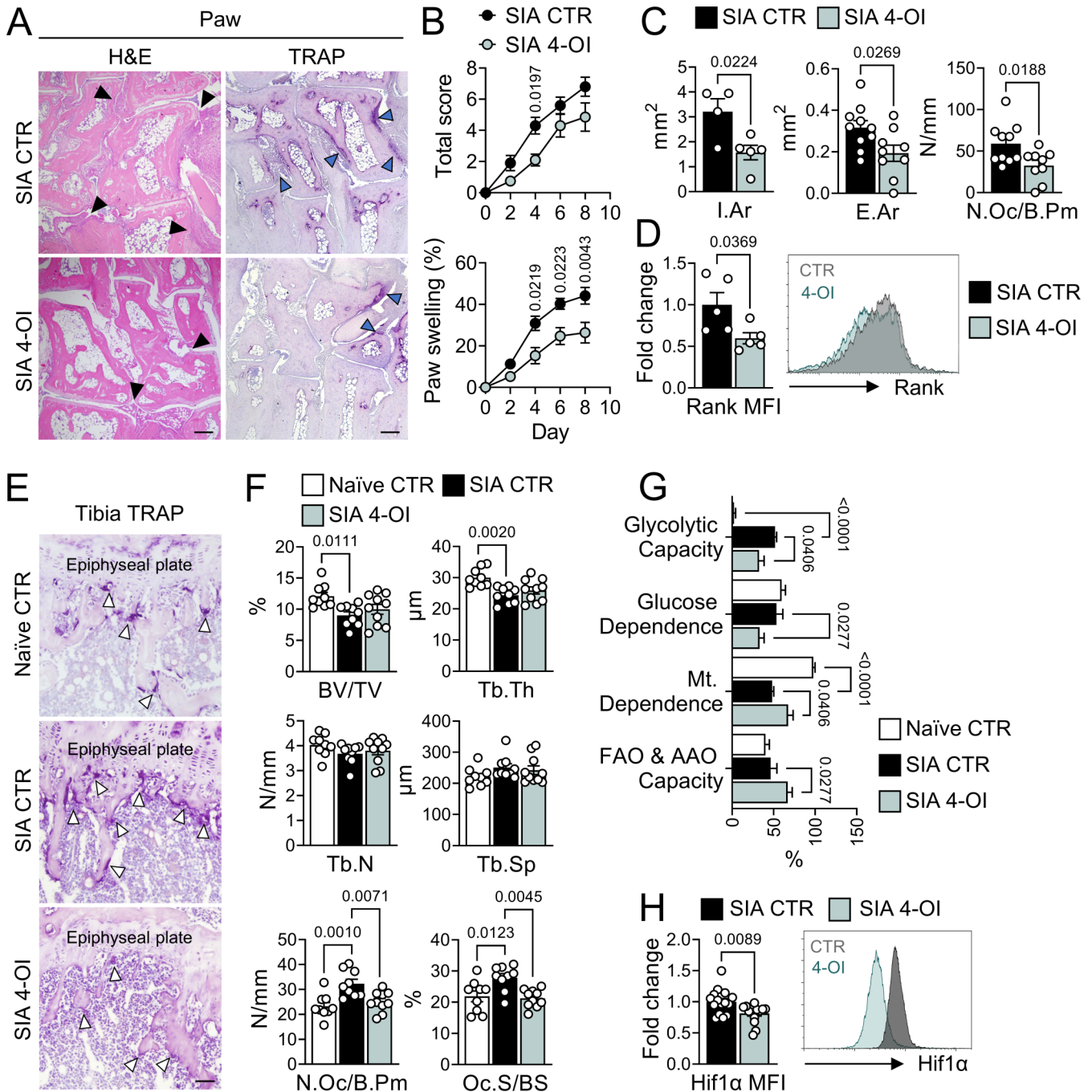


**Figure 6** 4-OI treatment mitigates inflammation and inflammation-mediated bone loss in experimental arthritis. (A) Representative pictures of hematoxylin and eosin (H&E) and tartrate-resistant acid phosphatase (TRAP)-stained paw tissue sections from 4-octyl-itaconate (4-OI) treated and control (CTR) wild-type (WT) mice with K/BxN serum-induced arthritis (SIA). Black arrow heads (H&E staining) indicate inflammation, blue arrow heads (TRAP staining) indicate eroded bone tissue with osteoclasts. Scale bar: 200  $\mu$ m. (B) Arthritis score and proportional paw swelling in 4-OI treated and CTR mice over the course of SIA (n=10). (C) Quantification of inflammation area (I.Ar), eroded bone area (E.Ar) and osteoclast number per bone perimeter (N.Oc/B.Pm) in H&E and TRAP-stained paw tissue sections of 4-OI treated and CTR mice with SIA (n=4–10). (D) Flow cytometry analysis of receptor activator of NF- $\kappa$ B (Rank) expression in CD45<sup>+</sup>CD11b<sup>+</sup>Ly6C<sup>hi</sup>CD115<sup>+</sup> osteoclast progenitors (OCPs) in the synovial ankle tissue of 4-OI treated and CTR mice with SIA, depicted as fold changes of the mean fluorescence intensity (MFI) in 4-OI treated as compared with CTR mice (n=5). (E) Representative images of TRAP-stained tibial sections from naïve CTR mice and SIA affected CTR and 4-OI treated mice. White arrow heads indicate osteoclasts. Scale bar: 50  $\mu$ m. (F) Quantification of bone volume per total volume (BV/TV), trabecular thickness (Tb.Th), trabecular number (Tb.N), trabecular space (Tb.Sp), number of osteoclasts per bone perimeter (N.Oc/B.Pm) and osteoclast surface per bone surface (Oc.S/BS) (n=9–10). (G) SCENITH analysis of metabolic parameters in OCPs from CTR mice with and without SIA and 4-OI treated mice with SIA (n=3–5). (H) Flow cytometry analysis of hypoxia-inducible factor (Hif)-1 $\alpha$  expression in synovial OCPs from 4-OI treated and CTR mice with SIA, depicted as fold changes of the MFI in 4-OI treated as compared with CTR mice (n=14–15). Data are shown as mean  $\pm$  SEM. Symbols represent individual mice. P values were determined by two-tailed Student's t-test for single comparisons and one-way or two-way ANOVA for multiple comparisons. ANOVA, analysis of variance.

## DISCUSSION

One of the major characteristics of RA is bone erosion, caused by a disruption of bone homeostasis in favour of increased OCP recruitment into the synovial compartment as well as enhanced osteoclast differentiation.<sup>9</sup> Recent research indicates that phenotypical and functional changes in cells that are involved in RA pathogenesis are associated with metabolic dysregulation that can promote disease progression. However, our understanding of the metabolic adaptations that occur in osteoclasts and OCPs in connection with RA is still limited. Our findings suggest that the metabolic signature linked to enhanced osteoclast differentiation in RA includes ATP production through Hif1 $\alpha$ -dependent aerobic glycolysis, mitochondrial hyperpolarisation, and the repurposing of mitochondria for ROS formation. Additionally, our data indicate that the Acod1-itaconate axis interferes with the metabolic alterations that drive osteoclast overactivation and consequently contribute to RA-associated bone loss.

In particular, we demonstrated that osteoclasts, derived from the PBMCs of RA patients and OCPs from inflamed ankle joints of mice with SIA exhibit increased dependence on glycolytic ATP production while being less dependent on mitochondrial energy production. In both, the human in vitro experiments and the SIA model, we observed that the glycolytic shift was associated with enhanced osteoclast differentiation. In human as well as murine in vitro cell culture we moreover observed a gradual upregulation of glycolytic activity over the course of osteoclastogenesis in the presence of normal oxygen levels, indicating that in this cell type glycolytic reprogramming is not merely an adaptation to the hypoxic environment of RA joints, but rather a crucial part of the differentiation process. Consistently, the inhibition of glycolytic metabolism at the initial stage of in vitro differentiation using 2-DG also blocked osteoclast development while the suppression of OXPHOS using the chemical uncoupler CCCP increased the number of mature, polynucleated osteoclasts. This is in line with previous reports on the importance of glycolytic metabolism for osteoclast maturation and resorptive function.<sup>15 41</sup>

Our results furthermore show that the mitochondrial enzyme Acod1 and its metabolic product itaconate serve as inhibitors of osteoclast differentiation by interfering with the metabolic reprogramming towards glycolysis. Thus, *ACOD1* mRNA expression in human PBMCs was negatively correlated with the number of mature osteoclasts. The itaconate-derivative 4-OI suppressed glycolytic activity and osteoclast differentiation in human and murine cells while the lack of itaconate in Acod1-deficient mice was associated with enhanced aerobic glycolysis and increased osteoclast numbers in vitro as well as in vivo. Acod1-deficiency accordingly resulted in exacerbated arthritis-associated bone loss but also aggravated inflammation. On the contrary, the therapeutic treatment of arthritic mice with 4-OI mitigated the inflammation as well as the bone degradation and caused a reduction in osteoclast cell numbers and the glycolytic capacity of ankle-resident OCPs. The ability of itaconate to alleviate inflammation in experimental arthritis models can be attributed to its well-known anti-inflammatory function. For instance, itaconate has been previously shown to inhibit LPS-mediated production of proinflammatory cytokines (interleukin (IL)6, IL12, IL18, IL1B and type I interferon (IFN)) by BMDMs<sup>20</sup> and to limit the innate and adaptive immune response in a murine model of systemic lupus erythematosus (SLE).<sup>42</sup> Our observations, demonstrating that itaconate levels in PBMCs from patients with RA were inversely correlated with RA disease activity and that *ACOD1* mRNA expression was reduced in active RA patients further

support the view that the Acod1-itaconate axis may have an impact on RA-associated inflammation. While the effect of Acod1 and 4-OI on local bone erosion and systemic bone loss in murine arthritis might, therefore, be partially caused by its influence on inflammation, our in vitro data as well as the increased osteoclast number in the tibial bone of naïve Acod1<sup>-/-</sup> mice clearly indicate an intrinsic function of Acod1 in osteoclastogenesis. In addition to that, 4-OI was previously shown to suppress bone loss in a non-inflammatory osteoporosis model, although this study did not address the mechanistic link between bone degradation and itaconate-mediated metabolic changes.<sup>23</sup>

Through further analysis of the role of Acod1 in osteoclast metabolism, we found that Acod1-mediated downregulation of aerobic glycolysis and osteoclast maturation depends on its ability to suppress the protein expression of Hif1 $\alpha$ , the inducible subunit of the transcription factor Hif1.<sup>31</sup> In the presence of sufficient oxygen levels, Hif1 $\alpha$  stabilisation can be achieved through ROS.<sup>43</sup> Here, we observed that Acod1-deficiency results in increased ROS levels on day 2 of osteoclast in vitro cell culture while ROS inhibition prevents both, Hif1 $\alpha$  upregulation and enhanced cell differentiation in the absence of Acod1. This is in line with previous reports on the ability of itaconate to suppress ROS formation<sup>44</sup> as well as with studies showing the importance of ROS for osteoclast development.<sup>45</sup>

Our results furthermore suggest that the increased ROS levels in Acod1-deficient cells could be explained by enhanced oxidation of succinate via the overactivated enzyme Sdh, consistently with previous reports on the ability of itaconate to suppress the enzymatic activity of Sdh.<sup>20</sup> Previous analyses of proinflammatory macrophages have revealed that enhanced activation of Sdh can mediate a repurposing of the mitochondrial electron transport chain from ATP generation to the production of excess amounts of ROS, which in turn can stabilise Hif1 $\alpha$  and induce a shift to aerobic glycolysis.<sup>46</sup> We propose that a similar mechanism of Sdh-dependent mitochondrial reprogramming might play an important role in osteoclast differentiation and is regulated through the Acod1-itaconate axis (figure 7).

Another metabolic characteristic of Acod1-deficient osteoclasts was enhanced mitochondrial fission. While a combination between mitochondrial fragmentation and a loss of membrane potential is commonly associated with mitochondrial dysfunction, fragmented mitochondria with hyperpolarised membrane potential are considered intact and are further defined by low oxygen consumption rates, low mitochondrial ATP production and high ROS production, which aligns with the metabolic phenotype of Acod1-deficient osteoclasts.<sup>37 47</sup> Besides that, mitochondrial fission was previously found to be linked to aerobic glycolysis and was moreover shown to directly facilitate the ability of T cells to undergo glycolytic reprogramming via the fission protein Drp1.<sup>48</sup> Drp1 is encoded by the gene *Dnm1l*, which we found to be upregulated in the absence of Acod1 and downregulated in response to 4-OI stimulation. How exactly the changes in mitochondrial morphology are interconnected with the metabolic state and differentiation ability of osteoclasts is, however, currently under investigation.

It is also not yet fully understood why the metabolic reprogramming towards aerobic glycolysis is beneficial for osteoclast differentiation. One possibility might be that osteoclast development belongs to the cellular processes that create an increased need for the cofactor NAD<sup>+</sup>, which is required for the generation of oxidised macromolecules, such as nucleotides and amino acids, histone deacetylation and calcium homeostasis.<sup>49-51</sup> If the demand for NAD<sup>+</sup> exceeds that for ATP, cells have been shown to undergo a shift to glycolytic ATP production to adapt to these

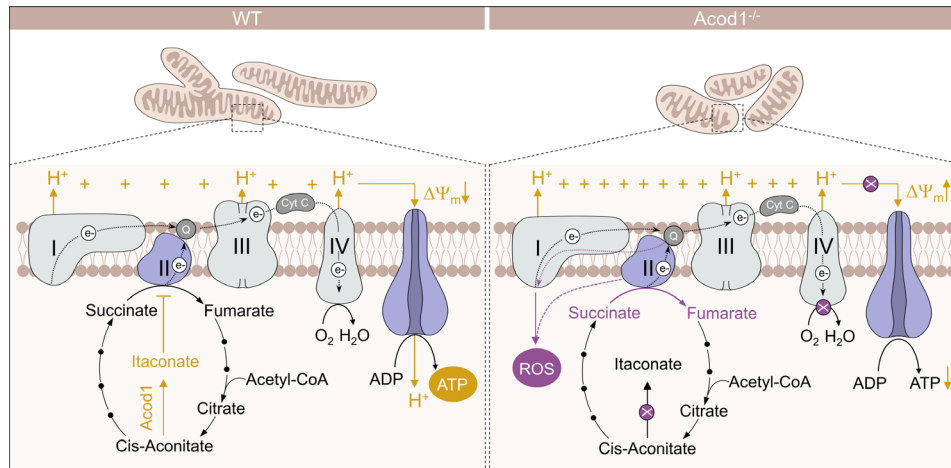


**Figure 7** Graphical illustration of Acod1-dependent mitochondrial pathways. Representation of electron transport chain dynamics comparing wild-type (WT) and aconitate decarboxylase 1-deficient (*Acod1*<sup>-/-</sup>) conditions. Acod1 catalyses the conversion of cis-aconitate to itaconate. Itaconate limits the activity of succinate dehydrogenase (complex II) within the electron transport chain, impeding the conversion of succinate into fumarate in the citric acid cycle. The lack of itaconate in the absence of Acod1 results in overactivation of Sdh, leading to repurposing of the electron transport chain for ROS production and is associated with mitochondrial hyperpolarisation and reduced mitochondrial adenosine triphosphate (ATP) production.

metabolic needs.<sup>52</sup> Another explanation could be the induction of epigenetic changes in response to altered acetyl coenzyme A (acetyl-CoA) levels caused by the metabolic reprogramming towards glycolysis, as previously observed in other cell types.<sup>53</sup> In fact, our RNAseq analysis revealed that the GO terms ‘epigenetic regulation of gene expression’ and ‘acetyl-CoA metabolic process’ were enriched among the genes that were regulated by *Acod1* and 4-OI in murine osteoclasts. Taken together, our data suggest that *Acod1* inhibits osteoclast differentiation and bone loss in RA due to its ability to suppress Sdh-mediated ROS production and Hif1 $\alpha$ -dependent aerobic glycolysis. The *Acod1*-itaconate axis might therefore serve as a promising target for the development of metabolic interventions to protect bone in arthritis.

### Limitations of the study

One limitation of our study is the reliance on in vitro differentiation techniques and examination of progenitor cells for analysing metabolic changes in osteoclasts, as mature osteoclasts cannot be extracted from bone or joint tissue. To mitigate this limitation, we combined murine and human in vitro experiments with analysis of tissue-resident OCPs in disease models, yielding consistent results.

### Author affiliations

<sup>1</sup>Department of Internal Medicine 3 – Rheumatology and Immunology, Friedrich-Alexander-University Erlangen-Nürnberg (FAU) and Universitätsklinikum Erlangen, Erlangen, Germany

<sup>2</sup>Deutsches Zentrum für Immuntherapie (DZI), Friedrich-Alexander-University Erlangen-Nürnberg (FAU) and Universitätsklinikum Erlangen, Erlangen, Germany

<sup>3</sup>Center for Regenerative Therapies Dresden (CRTD), Technische Universität (TU) Dresden, Dresden, Germany

<sup>4</sup>Department of Immune Modulation, Friedrich-Alexander-University Erlangen-Nürnberg (FAU) and Universitätsklinikum Erlangen, Erlangen, Germany

<sup>5</sup>Department of Ophthalmology, Friedrich-Alexander-University Erlangen-Nürnberg (FAU) and Universitätsklinikum Erlangen, Erlangen, Germany

<sup>6</sup>Department of Rheumatology, Zhejiang University – School of Medicine, Hangzhou, People’s Republic of China

<sup>7</sup>Division of Biochemistry, Department of Biology, Friedrich-Alexander-University Erlangen-Nürnberg (FAU), Erlangen, Germany

<sup>8</sup>Institute of Experimental and Clinical Pharmacology and Toxicology, Friedrich-Alexander-University Erlangen-Nürnberg (FAU), Erlangen, Germany

**Acknowledgements** We thank Daniela Weidner, Jule Lindörfer, Franceska Jelas, Christine Zech, Barbara Happich and Nicole Berndt for great technical assistance. The authors thank Dr. Wolfgang Baum for the generation of K/BxN serum.

**Contributors** KK acquired funding, designed the study, performed experiments, interpreted results and wrote the manuscript. DA, ST, SK, MLP and ML performed experiments, collected and interpreted data. DR and AS provided expertise and helped to establish the CRISPR/ Cas9-mediated gene knockout experiments. JH, AG and MF provided expertise and performed mass spectrometry analyses. SR helped to establish the hTNFtg arthritis model. XM helped to establish the SCENITH experiments. AG performed transmission electron microscopy analyses. GS and AB acquired funding, directed the study and wrote the manuscript. AB is responsible for the overall content as guarantor. All authors read and commented on the manuscript.

**Funding** This study was supported by the Interdisciplinary Center for Clinical Research (IZKF) grant J76, J90 and A77, the Collaborative Research Centre 1181 project A01, the Collaborative Research Center/Transregio 369 project B03, the German Research Foundation grant FOR2886 TP02, TRR/CRC369 DIONE—501752319 project A02, INST90/1048-1 FUGG, GRK2599-FAIR and GRK2740-immunomicrotopo, the European Research Council Consolidator Grant LS4-ODE, the Leibniz Award of the DFG (to GS) and the Synergy Grant 4D Nanoscope.

**Competing interests** None declared.

**Patient and public involvement** Patients and/or the public were not involved in the design, or conduct, or reporting, or dissemination plans of this research.

**Patient consent for publication** Not applicable.

**Ethics approval** All mouse experiments were performed according to the rules and regulations of the animal facility FPZ (Franz-Penzoldt-Zentrum, Erlangen) and approved by the ethical committee of the government of Unterfranken, Würzburg, Germany. All analyses of human material were approved by the institutional review board (IRB) of the University Clinic Erlangen and were in accordance with the Declaration of Helsinki—Ethical Principles for Medical Research Involving Human Subjects.

**Provenance and peer review** Not commissioned; externally peer reviewed.

**Data availability statement** Data are available on reasonable request. All sequencing data have been deposited in the National Centre for Biotechnology Information Gene Expression Omnibus (GEO). The accession number for the sequencing data reported in this paper is GEO: GSE237504.

**Supplemental material** This content has been supplied by the author(s). It has not been vetted by BMJ Publishing Group Limited (BMJ) and may not have been peer-reviewed. Any opinions or recommendations discussed are solely those of the author(s) and are not endorsed by BMJ. BMJ disclaims all liability and responsibility arising from any reliance placed on the content. Where the content includes any translated material, BMJ does not warrant the accuracy and reliability of the translations (including but not limited to local regulations, clinical guidelines, terminology, drug names and drug dosages), and is not responsible for any error and/or omissions arising from translation and adaptation or otherwise.

**Open access** This is an open access article distributed in accordance with the Creative Commons Attribution Non Commercial (CC BY-NC 4.0) license, which permits others to distribute, remix, adapt, build upon this work non-commercially, and license their derivative works on different terms, provided the original work is properly cited, appropriate credit is given, any changes made indicated, and the use is non-commercial. See: <http://creativecommons.org/licenses/by-nc/4.0/>.

#### ORCID iDs

Mireia Llerins Perez <http://orcid.org/0000-0001-5323-0609>

Simon Rauber <http://orcid.org/0000-0001-8306-9334>

Georg Schett <http://orcid.org/0000-0001-8740-9615>

Aline Bozec <http://orcid.org/0000-0001-8174-2118>

#### REFERENCES

- Safiri S, Kolahi AA, Hoy D, et al. Global, regional and national burden of rheumatoid arthritis 1990-2017: a systematic analysis of the Global Burden of Disease Study 2017. *Ann Rheum Dis* 2019;78:1463–71.
- McInnes IB, Schett G. The pathogenesis of rheumatoid arthritis. *N Engl J Med* 2011;365:2205–19.
- Weyand CM, Goronzy JJ. Immunometabolism in early and late stages of rheumatoid arthritis. *Nat Rev Rheumatol* 2017;13:291–301.
- Muz B, Khan MN, Kiriakidis S, et al. The role of hypoxia and HIF-dependent signalling events in rheumatoid arthritis. *Arthritis Res Ther* 2009;11:201.
- Hu Z, Zhao TV, Huang T, et al. The transcription factor Rfx5 coordinates antigen-presenting function and resistance to nutrient stress in synovial Macrophages. *Nat Metab* 2022;4:759–74.
- Yang Z, Shen Y, Oishi H, et al. Restoring oxidant signaling suppresses proarthritogenic T cell Effector functions in rheumatoid arthritis. *Sci Transl Med* 2016;8:331ra38.
- Zeisbrich M, Yanes RE, Zhang H, et al. Hypermetabolic macrophages in rheumatoid arthritis and coronary artery disease due to glycogen synthase kinase 3B inactivation. *Ann Rheum Dis* 2018;77:1053–62.
- Garcia-Carbonell R, Divakaruni AS, Lodi A, et al. Critical role of glucose metabolism in rheumatoid arthritis fibroblast-like synoviocytes. *Arthritis Rheumatol* 2016;68:1614–26.
- Schett G, Gravalles E. Bone erosion in rheumatoid arthritis: mechanisms, diagnosis and treatment. *Nat Rev Rheumatol* 2012;8:656–64.
- Węgierska M, Dura M, Blumfield E, et al. Osteoporosis diagnostics in patients with rheumatoid arthritis. *Rheumatologia* 2016;54:29–34.
- Adamopoulos IE. Inflammation in bone physiology and pathology. *Curr Opin Rheumatol* 2018;30:59–64.
- Bromley M, Woolley DE. Chondroclasts and osteoclasts at subchondral sites of erosion in the rheumatoid joint. *Arthritis Rheum* 1984;27:968–75.
- Mbalaviele G, Novack DV, Schett G, et al. Inflammatory osteolysis: a conspiracy against bone. *J Clin Invest* 2017;127:93356:2030–9.
- Li B, Lee W-C, Song C, et al. Both aerobic glycolysis and mitochondrial respiration are required for osteoclast differentiation. *FASEB J* 2020;34:11058–67.
- Srivastava RK, Sapra L, Mishra PK. Osteometabolism: metabolic alterations in bone Pathologies. *Cells* 2022;11:3943.
- Michelucci A, Cordes T, Ghelfi J, et al. Immune-responsive gene 1 protein links metabolism to immunity by catalyzing Itaconic acid production. *Proc Natl Acad Sci U S A* 2013;110:7820–5.
- Degrandi D, Hoffmann R, Beuter-Gunia C, et al. The proinflammatory cytokine-induced Irg1 protein associates with mitochondria. *J Interferon Cytokine Res* 2009;29:55–67.
- Wu R, Chen F, Wang N, et al. Acd1 in Immunometabolism and disease. *Cell Mol Immunol* 2020;17:822–33.
- Ahmed SMU, Luo L, Namani A, et al. NRF2 signaling pathway: pivotal roles in inflammation. *Biochim Biophys Acta Mol Basis Dis* 2017;1863:585–97.
- Lamproulou V, Sergushichev A, Bambouskova M, et al. Itaconate links inhibition of succinate dehydrogenase with macrophage metabolic remodeling and regulation of inflammation. *Cell Metab* 2016;24:158–66.
- Liao S-T, Han C, Xu D-Q, et al. 4-Octyl Itaconate inhibits aerobic glycolysis by targeting GAPDH to exert anti-inflammatory effects. *Nat Commun* 2019;10:5091.
- Mills EL, Ryan DG, Prag HA, et al. Itaconate is an anti-inflammatory metabolite that activates Nrf2 via Alkylation of Keap1. *Nature* 2018;556:113–7.
- Sun X, Zhang B, Pan X, et al. Octyl Itaconate inhibits osteoclastogenesis by suppressing HRD1 and activating NRF2 signaling. *FASEB J* 2019;33:12929–40.
- Aletaha D, Neogi T, Silman AJ, et al. Rheumatoid arthritis classification criteria: an American college of rheumatology/European League against rheumatism collaborative initiative. *Arthritis & Rheumatism* 2010;62:2569–81.
- Keffer J, Probert L, Cazlaris H, et al. Transgenic mice expressing human tumour necrosis factor: a predictive genetic model of arthritis. *EMBO J* 1991;10:4025–31.
- Korganow AS, Ji H, Mangialaio S, et al. From systemic T cell self-reactivity to organ-specific autoimmune disease via immunoglobulins. *Immunity* 1999;10:451–61.
- Chen Z, Andreev D, Oeser K, et al. Th2 and eosinophil responses suppress inflammatory arthritis. *Nat Commun* 2016;7:11596.
- Argüello RJ, Combes AJ, Char R, et al. SCENITH: A flow cytometry-based method to functionally profile energy metabolism with single-cell resolution. *Cell Metab* 2020;32:1063–75.
- Zhang D, Li J, Wang F, et al. 2-Deoxy-D-glucose targeting of glucose metabolism in cancer cells as a potential therapy. *Cancer Letters* 2014;355:176–83.
- Kasianowicz J, Benz R, McLaughlin S. The kinetic mechanism by which CCCP (carbonyl cyanide M-Chlorophenylhydrazone) transports protons across membranes. *J Membr Biol* 1984;82:179–90.
- Hu C-J, Wang L-Y, Chodosh LA, et al. Differential roles of hypoxia-inducible factor 1Alpha (HIF-1Alpha) and HIF-2Alpha in hypoxic gene regulation. *Mol Cell Biol* 2003;23:9361–74.
- Ivan M, Kondo K, Yang H, et al. Hif1alpha targeted for VHL-mediated destruction by proline hydroxylation: implications for O2 sensing. *Science* 2001;292:464–8.
- Jaakkola P, Mole DR, Tian YM, et al. Targeting of HIF-1alpha to the von Hippel-Lindau Ubiquitylation complex by O2-regulated Prolyl hydroxylation. *Science* 2001;292:468–72.
- Yu F, White SB, Zhao Q, et al. HIF-1Alpha binding to VHL is regulated by stimulus-sensitive Proline hydroxylation. *Proc Natl Acad Sci U S A* 2001;98:9630–5.
- Ho VT, Bunn HF. Effects of transition metals on the expression of the erythropoietin gene: further evidence that the oxygen sensor is a Heme protein. *Biochem Biophys Res Commun* 1996;223:175–80.
- Oikawa T, Oyama M, Kozuka-Hata H, et al. Tks5-dependent formation of circumferential podosomes/Invadopodia mediates cell-cell fusion. *J Cell Biol* 2012;197:553–68.
- Liesa M, Shirihai OS. Mitochondrial dynamics in the regulation of nutrient utilization and energy expenditure. *Cell Metab* 2013;17:491–506.
- Sun SY. N-Acetylcysteine, reactive oxygen species and beyond. *Cancer Biol Ther* 2010;9:109–10.
- Cordes T, Wallace M, Michelucci A, et al. Immuno-responsive gene 1 and Itaconate inhibit succinate dehydrogenase to modulate intracellular Succinate levels. *J Biol Chem* 2016;291:14274–84.
- Tannahill GM, Curtis AM, Adamik J, et al. Succinate is an inflammatory signal that induces IL-1Beta through HIF-1Alpha. *Nature* 2013;496:238–42.
- Taubmann J, Krishnacoumar B, Böhm C, et al. Metabolic reprogramming of osteoclasts represents a therapeutic target during the treatment of osteoporosis. *Sci Rep* 2020;10:21020.
- Blanco LP, Patino-Martinez E, Nakabo S, et al. Modulation of the Itaconate pathway attenuates murine lupus. *Arthritis Rheumatol* 2022;74:1971–83.
- Hamanaka RB, Weinberg SE, Reczek CR, et al. The mitochondrial respiratory chain is required for organismal adaptation to hypoxia. *Cell Rep* 2016;15:451–9.
- Li Y, Chen X, Zhang H, et al. 4-Octyl Itaconate Alleviates Lipopolysaccharide-induced acute lung injury in mice by inhibiting oxidative stress and inflammation
- Srinivasan S, Koenigstein A, Joseph J, et al. Role of mitochondrial reactive oxygen species in osteoclast differentiation. *Ann N Y Acad Sci* 2010;1192:245–52.
- Mills EL, Kelly B, Logan A, et al. Succinate dehydrogenase supports metabolic repurposing of mitochondria to drive inflammatory macrophages. *Cell* 2016;167:457–70.
- Nagdas S, Kashatus DF. The interplay between oncogenic signaling networks and mitochondrial dynamics. *Antioxidants (Basel)* 2017;6:33.
- Buck MD, O'Sullivan D, Klein Geltink RI, et al. Mitochondrial dynamics controls T cell fate through metabolic programming. *Cell* 2016;166:63–76.
- Hosios AM, Vander Heiden MG. The redox requirements of proliferating mammalian cells. *J Biol Chem* 2018;293:7490–8.
- Cantó C, Menzies KJ, Auwerx J. Metabolism and the control of energy homeostasis: a balancing act between mitochondria and the nucleus. *Cell Metab* 2015;22:31–53.
- Ying W. NAD<sup>+</sup>/NADH and NADP<sup>+</sup>/NADPH in cellular functions and cell death: regulation and biological consequences. *Antioxid Redox Signal* 2008;10:179–206.
- Luengo A, Li Z, Gui DY, et al. Increased demand for NAD(+) relative to ATP drives aerobic Glycolysis. *Molecular Cell* 2021;81:691–707.
- Moussaieff A, Rouleau M, Kitsberg D, et al. Glycolysis-mediated changes in acetyl-CoA and Histone Acetylation control the early differentiation of embryonic stem cells. *Cell Metab* 2015;21:392–402.